공학박사 학위논문

DEVELOPMENT OF ADDITIONAL MASTER INTERFACES FOR ENHANCED FUNCTION OF LAPAROSCOPIC SURGICAL ROBOT SYSTEM AND ITS APPLICATIONS

복강경 수술 로봇 시스템의 활용도 향상을 위한 추가적인 마스터 인터페이스 개발과 이를 이용한 응용 시스템 개발 연구

2017 년 8 월

서울대학교 대학원

협동과정 바이오엔지니어링 전공

김 명 준

DEVELOPMENT OF ADDITIONAL MASTER INTERFACES FOR ENHANCED FUNCTION OF LAPAROSCOPIC SURGICAL ROBOT SYSTEM AND ITS APPLICATIONS

복강경 수술 로봇 시스템의 활용도 향상을 위한 추가적인 마스터 인터페이스 개발과 이를 이용한 응용 시스템 개발 연구

지도교수 김 성 완

이 논문을 공학박사 학위논문으로 제출함

2017 년 7 월

서울대학교 대학원
협동과정 바이오엔지니어링 전공
김 명 준

김명준의 공학박사 학위논문을 인준함

2017 년 6 월

위 원 장	박 광 석	(인)
부위원장	김 성 완	(인)
위 원	이 정 찬	(인)
위 원	김 유 단	(인)
위 원	이 두 용	(인)

Ph. D. Dissertation

DEVELOPMENT OF ADDITIONAL MASTER INTERFACES FOR ENHANCED FUNCTION OF LAPAROSCOPIC SURGICAL ROBOT SYSTEM AND ITS APPLICATIONS

BY

MYUNGJOON KIM

JULY 2017

INTERDISCIPLINARY PROGRAM IN BIOENGINEERING

THE GRADUATE SCHOOL

SEOUL NATIONAL UNIVERSITY

DEVELOPMENT OF ADDITIONAL MASTER INTERFACES FOR ENHANCED FUNCTION OF LAPAROSCOPIC SURGICAL ROBOT SYSTEM AND ITS APPLICATIONS

BY

MYUNGJOON KIM

INTERDISCIPLINARY PROGRAM IN BIOENGINEERING

THE GRADUATE SCHOOL

SEOUL NATIONAL UNIVERSITY

THIS DISSERTATION IS APPROVED FOR THE DEGREE OF DOCTOR OF PHILOSOPHY

JUNE 2017

DOCTORAL COMMITTEE:

Chairman	*Kwang Suk Park, Ph. D.*
Vice Chairman	*Sungwan Kim, Ph. D.*
Member	*Jung Chan Lee, Ph. D.*
Member	*Youdan Kim, Ph. D.*
Member	*Doo Yong Lee, Ph. D.*

서울대학교총장 귀하

Abstract

DEVELOPMENT OF ADDITIONAL MASTER INTERFACES FOR ENHANCED FUNCTION OF LAPAROSCOPIC SURGICAL ROBOT SYSTEM AND ITS APPLICATIONS

By

Myungjoon Kim

Interdisciplinary Program in Bioengineering
The Graduate School
Seoul National University

Robot-assisted laparoscopic surgery offers several advantages compared to open surgery and conventional minimally invasive surgery. However, important issues which need to be resolved are the complexity of current operation room environment for laparoscopic robotic surgery and demand for a larger operation room. To overcome these issues, additional interfaces based on Hands-On-Throttle-And-Stick (HOTAS) concept which can be simply attached and integrated with master interface of da Vinci surgical robot system were proposed. HOTAS controller is widely used for flight control in the aerospace field which can manipulate hundreds of functions and provide feedback to the pilot on flight conditions. The implementation of HOTAS controller significantly reduced the complexity of flights and reduced the number of pilots required in a cockpit from two to one.

In this study, to provide above benefits to the operation room for robotic laparoscopic surgery, two types of additional interfaces are proposed. Proposed additional interfaces can be easily manipulated by the surgeon's index finger, which is currently operated only by finger clutch buttons, and therefore enable the surgeon to use multiple functions. Initially, a novel master interface (NMI) was developed. The NMI mainly consists of a 9-way switch and a microprocessor with a wireless communication module. Thus, the NMI can be also regarded as a 9-way compact HOTAS. The performance test, latency, and power consumption of the developed NMI were verified by repeated experiments. Then, an improved novel master interface (iNMI) was developed to provide more intuitive and convenient manipulation. The iNMI was developed based on a capacitive touch sensor array and a wireless microprocessor to intuitively reflect the surgeon's decision. Multiple experiments were performed to evaluate the iNMI performance in terms of performance test, latency, and power consumption.

In addition, two application systems based on Surgical-Operation-By-Wire (SOBW) concept are proposed in this research to enhance the function of laparoscopic surgical robot system based on clinical needs that are stated below. The size of the additional interface is small enough to be easily installed to the master tool manipulators (MTMs) of da Vinci research kit (dVRK), which was used as an operation robot arm system, to maximize convenience to the surgeon when using the additional interfaces to simultaneously manipulate the application systems with the MTMs.

Firstly, a robotic assistant that can be simultaneously manipulated via a wireless controller is proposed to allow the surgeon to control the assistant instrument. This approach not only decreases surgeon fatigue by eliminating communication process with assistants, but also resolves collision between the operation robot arms and the assistant instruments that can be caused by an inexperienced assistant or miscommunication and misaligned intent between the surgeon and the assistant. The system comprises two additional interfaces,

a surgical instrument with a gripper actuated by a micromotor and a 6-axis robot arm. The gripping force of the surgical instrument was comparable to that of conventional systems and was consistent even after 1,000 times of gripping motion. The workspace was calculated to be 8,397.4 cm^3. Recruited volunteers were able to execute the simple peg task within the cut-off time and successfully performed the *in vitro* test.

Secondly, a wirelessly controllable stereo endoscope system which enables simultaneous control with the operating robot arm system is proposed. This is able to remove any discontinuous surgical flow that occurs when the control is swapped between the endoscope system and the operating robot arm system, and therefore prevent problems such as increased operation time, collision among surgical instruments, and injury to patients. The proposed system consists of two additional interfaces, a four-degrees of freedom (4-DOFs) endoscope control system (ECS) and a simple three-dimensional (3D) endoscope. The 4-DOFs ECS consists of four servo motors and employs a two-parallel link structure to provide translational and fulcrum point motions to the simple 3D endoscope. The workspace was calculated to be 20,378.3 cm^3, which exceeds the reference workspace. The novice volunteers were able to successfully execute the modified peg transfer task.

Throughout the various verifications, it has been confirmed that the proposed interfaces could make the surgical robot system more efficiently by overcoming its several limitations.

Keywords: Laparoscopic surgical robot, Additional master interfaces, Hands-on-throttle-and-stick, Robotic assitant, Stereo endoscpoe system, Surgical-operation-by-wire.

Student number: 2013-21032

List of Tables

Table 1.1 Strengths and limitations for surgeries operated by humans and robots 2

Table 1.2 Advantages and disadvantages of robotic and non-robotic laparoscopic surgery 3

Table 2.1 Forward kinematics of the system (D-H parameters) 45

Table 3.1 Repeated experimental results of gripping force measurements 60

Table 3.2 System specifications of the robotic assistant 65

Table 3.3 Execution time of block transfer task 69

Table 3.4 System specifications of the 4-DOFs ECS 80

Table 3.5 Execution time of modified peg transfer task using the NMI 84

Table 3.6 Execution time of modified peg transfer task using the iNMI 88

List of Figures

Figure 1.1 (a) The Puma 560. (b) The ROBODOC. (c) The Automated Endoscopic System for Optimal Positioning (AESOP) robot. (d) The Zeus surgical robot system. 6

Figure 1.2 (a) The da Vinci surgical robot system. (b) The da Vinci surgical robot system's end-effectors, EndoWrists. 7

Figure 1.3 (a) Robotic surgery performed by more than one surgeon. (b) Actual operation room environment..... 9

Figure 1.4 (a) Hands-On-Throttle-And-Stick (HOTAS) used for flight control in the aerospace field. (b) Target position for installing additional master interfaces in current laparoscopic surgical robot system. 10

Figure 2.1 Layer information of proposed novel master interface (NMI). 23

Figure 2.2 Developed NMI. (a) Front and back side of the NMI. (b) The NMI attached on the MTM of the dVRK system using the special holder. (c) Usage of the index finger to operate finger clutch and the NMI. 24

Figure 2.3 Mapping information between the NMI and the surgical instrument. (a) Left NMI. (b) Right NMI. 25

Figure 2.4 Developed improved novel master interface (iNMI). (a) Front and back sides of the iNMI. (b) Case and silicone top layer to protect the iNMI. (c) The iNMI attached on the MTM of the dVRK system using the special holder. 28
Figure 2.5 Design of proposed touch sensors array. 29
Figure 2.6 Layer information of the iNMI. 30
Figure 2.7 Mapping information of the iNMI. The fulcrum point motion can be achieved using one of the two iNMIs while the translational motion and rolling motion can only be performed by combination of two iNMIs' gesture input. 33
Figure 2.8 Control flow of the proposed robotic assistant driven by the surgeon's intention. Software integration is based on the LabVIEW® software. 36
Figure 2.9 Overall system of the da Vinci research kit (dVRK). (a) Controllers. (b) Stereo viewer. (c) Master tool manipulators (MTMs). (d) Foot pedal. (e) Two webcams for providing images. (f) Patient side manipulators (PSMs). dVRK is used as operation surgical robot system in this research. 38
Figure 2.10 Design of the proposed surgical instrument. The gripping motion is achieved by converting the micro motor's rotation motion into linear motion by male and female screw and linking the gripper with the female screw through the linkage.

The length and the diameter of the surgical instrument is designed as 300 mm and 6 mm, respectively. 41

Figure 2.11 Surgical instrument manufactured using aluminum. (a) The surgical instrument without the upper outer shell. Actual position of the micro motor, male and female screw, linkage, and the gripper is shown. (b) The surgical instrument with the upper outer shell. 42

Figure 2.12 Joint information of the 6-degrees of freedom (DOFs) external robot arm. The fulcrum point motion and the translational motion of the surgical instrument are achieved by complex combination from *J1* to *J5*. The surgical instrument's rolling motion is achieved by *J6*. 44

Figure 2.13 Kinematic structure of the system. 48

Figure 2.14 Control flow of the proposed surgical robot system driven by the surgeon's intention. Software integration is based on the LabVIEW® software. 50

Figure 2.15 Simple three-dimensional (3D) endoscope manufactured using 3D printing technique. Two complementary metal-oxide-semiconductor (CMOS) camera modules are used for reconstructing stereo view. 6 Built-in light-emitting diodes (LEDs) of each module is used as light source. The tip of the endoscope is developed to have 30 degrees to procure a wide

range of view. The length and the diameter of the surgical instrument is designed as 300 mm and 10 mm, respectively. 53

Figure 2.16 4-DOFs endoscope control system (ECS). The fulcrum point motion is achieved by *J1* and *J2* with its two-parallel link structure. The translational motion and rolling motion are accomplished by *J3* and *J4*, respectively. 55

Figure 3.1 Experimental results of gripping force compliant with position of the micro motor. The experiments repeated 10 times and the standard deviation is plotted as error bar. The interval of the position of the micro motor was 0.05 revs. 61

Figure 3.2 Workspace of the proposed robotic assistant. 64

Figure 3.3 System setup for the peg transfer task using fundamental of laparoscopic surgery (FLS). 68

Figure 3.4 Setup for the *in vitro* test of semi-automatic resected object removal. (a) Overall system setup. (b) Built-in magnet of the surgical instrument to generate magnetic field. (c) Magnetic sensor with its controller board within the special housing. (d) Developed simulated trocar used in the *in vitro* test. 71

Figure 3.5 Control flow of the automatic mode needed in the *in vitro* test..... 74

Figure 3.6 Stereo calibration and rectification processes. (a) Stereo calibration process. (b) Stereo rectification process. (c)

Calibrated and rectified images with effective area enclosed in a pink box. 76

Figure 3.7 Comparison between original images and final images. (a) Original images obtained. (b) Final images after stereo calibration, rectification, and reconstruction. 77

Figure 3.8 Workspace of the proposed 4-DOFs ECS. 79

Figure 3.9 System setup for the modified peg transfer task. Modified peg transfer board was developed and used for the task to evaluate the overall performance of the proposed system. 83

Figure 4.1 Workspace analysis of the proposed robotic assistant with regard to PSMs. (a) An extreme condition to the robotic assistant's workspace. (b) Calculated workspace in the extreme condition. 95

Figure 4.2 Comparison between peg transfer task results using the NMI and iNMI (Error bar stands for standard deviation). 99

Contents

Abstract ..... **i**

List of Tables ..... **iv**

List of Figures ..... **vi**

Contents ..... **xi**

1. Introduction **1**

1.1. Robotic Laparoscopic Surgery 1

1.2. Objectives and Scope 8

1.2.1. Additional Master Interfaces 14

1.2.2. Application Systems 15

2. Materials and Methods **20**

2.1. Additional Master Interfaces 20

2.1.1. Novel Master Interface: 9-way Compact Hands-On-Throttle-And-Stick 20

2.1.2. improved Novel Master Interface: Capacitive Touch Type Compact Hands-On-Throttle-And-Stick 26

2.2. Application Systems 34

2.2.1. Robotic Assistant 34

2.2.2. Stereo Endoscope System 49

3. Results **56**

3.1. .....Novel Master Interface with Application Systems 56

3.1.1. Novel Master Interface..... 56

3.1.2. Robotic Assistant 58

3.1.3. ..... Novel Master Interface with Robotic Assistant 66

3.1.4. Stereo Endoscope System 75

3.1.5. Novel Master Interface with Stereo Endoscope System 81

3.2. improved Novel Master Interface with Application Systems ... 85

3.2.1. improved Novel Master Interface 85

3.2.2. improved Novel Master Interface with Stereo Endoscope System 88

4. Discussion **89**

5. Conclusion **100**

References **103**

Abstract in Korean **115**

Acknowledgement **118**

1. Introduction

1.1. Robotic Laparoscopic Surgery

Conventional minimally invasive surgery (MIS) has become one of the most advocated surgical operation approach because it offers benefits such as low blood loss, reduced time to drain removal, shorter hospital stay, better pain score, fewer follow-ups, smaller incision, and reduced complication rate than open surgery [1, 2]. However, MIS has the following disadvantages: because the degrees of freedom (DOFs) of the surgical instrument is low, surgical operations such as suturing are difficult for inexpert surgeons to perform, resulting in the need for highly-trained surgeons to perform surgical operations [3, 4]. Consequently, robot-assisted laparoscopic surgery has been developed to overcome the limitations of both types of surgeries [5-8]. The strengths and limitations for surgeries operated by humans and robots are presented in Table 1.1 [9]. The advantages and disadvantages of robotic and non-robotic laparoscopic surgery are summarized in Table 1.2 [6].

Table 1.1 Strengths and limitations for surgeries operated by humans and robots [9]

	Humans	Robots
Strengths	- Strong hand-eye coordination - Dexterous (at human scale) - Flexible and adaptable - Can integrate extensive and diverse information - Able to use qualitative information - Good judgment - Easy to instruct and debrief	- Good geometric accuracy - Stable and untiring - Can be designed for a wide range of scales - May be sterilized - Resistant to radiation and infection - Can use diverse sensors (force, etc.) in control
Limitations	- Limited dexterity outside natural scale - Prone to tremor and fatigue - Limited geometric accuracy - Limited ability to use quantitative information - Limited sterility - Susceptible to radiation and infection	- Poor judgment - Limited dexterity and hand-eye coordination - Limited to relatively simple procedures - Expensive - Technology in flux

Table 1.2 Advantages and disadvantages of robotic and non-robotic laparoscopic surgery [6]

	Conventional laparoscopic surgery	Robotic laparoscopic surgery
Advantages	- Well-developed technology - Affordable and ubiquitous - Proven efficacy	- 3-D visualization - Improved dexterity - High degrees of freedom - Elimination of fulcrum effect - Elimination of physiologic tremors - Ability to scale motions - Micro-anastomoses possible - Tele-surgery - Ergonomic position
Disadvantages	- Loss of touch sensation - Loss of 3-D visualization - Compromised dexterity - Limited degrees of motion - The fulcrum effect - Amplification of physiologic tremors	- Absence of touch sensation - Expensive - High start-up cost - May require extra staff to operate and big operating space - Increased operation time

Introduction of the surgical robot has resulted in benefits such as reduced blood loss, better pain score, reduced time to drain removal, shorter hospital stay, reduced complication rate, and fewer follow-ups, even compared with conventional MIS [1]. Furthermore, it facilitates improved surgical precision, better visualization, and more intuitive and ergonomic instrument control—resulting in shorter learning curves for surgeons [10]. The pioneer in robotic surgery was the Puma 560, which was used for neurosurgical biopsies in 1985 and showed greater precision [6, 11]. The ROBODOC was then developed for hip replacement surgery and it was the first FDA approved surgical robot system [12, 13]. After this, National Air and Space Administration (NASA) and Stanford Research Institute (SRI) proposed the concept of tele-surgery based on robotic technology and developed dexterous tele-operated surgical robot in 1990s [12]. The Integrated Surgical Systems, which is the predecessor of Intuitive Surgical, successfully developed the da Vinci laparoscopic surgical robot system following by licensing the SRI Green Telepresence Surgery System after the Automated Endoscopic System for Optimal Positioning (AESOP) robot was marketed [6, 14]. In this time, the Zeus (Computer Motion Inc., Santa Barbara, CA, USA) surgical robot system was also developed. Yet, it was phased out in the early 2000s as the Intuitive Surgical and Computer Motion merged into a single company [15]. Fig. 1.1 shows the above-mentioned surgical robot systems [16-18].

The da Vinci (Intuitive Surgical, Inc., Sunnyvale, CA, USA) surgical robot system, which is the market-leading surgical robot system, can be shown in

Fig. 1.2-(a). This system, which has to be controlled by a skillful surgeon, has improved safety and efficacy for laparoscopic surgery. When the surgeon control the master interface in work-console, the patient side manipulator and EndoWrist is able to mimic the movements of the surgeon's motion. The number of operations performed with the da Vinci rapidly increases every year [19]. Over the last decade, more than 1.5 million laparoscopic surgical operations, including gynecologic, cardiac, urology, thoracic, head & neck, and general surgery, have been performed worldwide using the da Vinci robot [19]. da Vinci surgical robot system has greatly reduced the number of open surgeries for common operation such as hysterectomy and prostatectomy [19, 20].

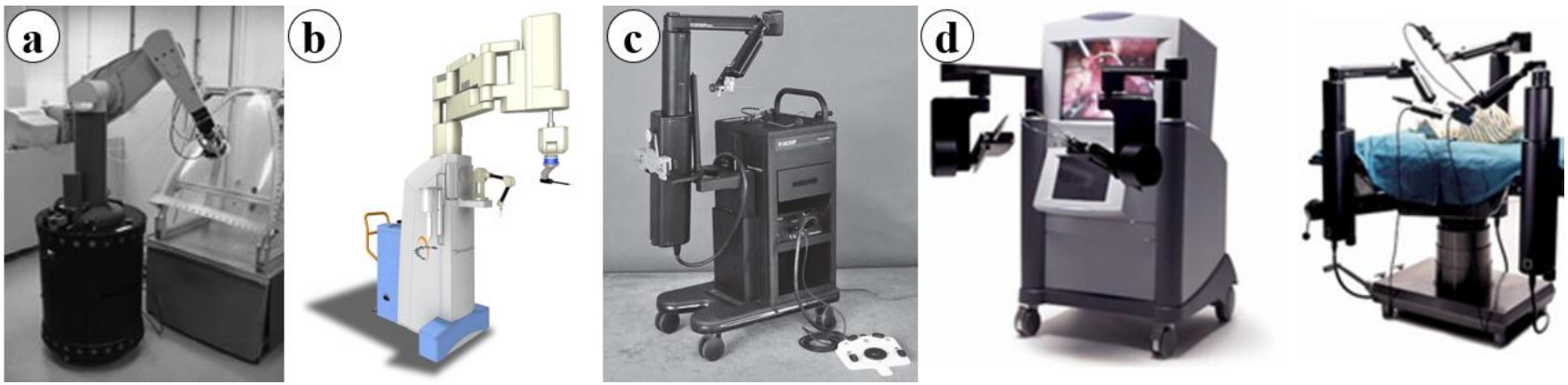

Fig. 1.1 (a) The Puma 560 [16]. (b) The ROBODOC [16]. (c) The Automated Endoscopic System for Optimal Positioning (AESOP) robot [17]. (d) The Zeus surgical robot system [18].

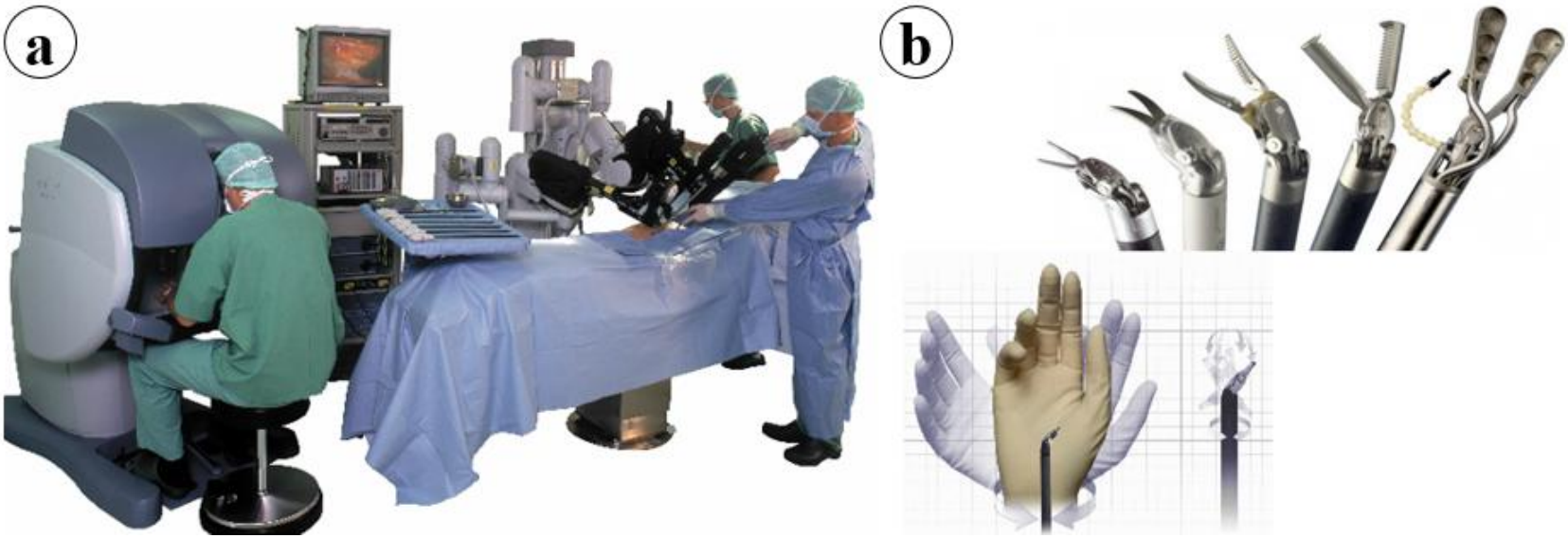

Fig. 1.2 (a) The da Vinci surgical robot system [21]. (b) The da Vinci surgical robot system's end-effectors, EndoWrists [22].

1.2. Objectives and Scope

The da Vinci surgical robot system (Intuitive Surgical, Inc., Sunnyvale, CA, USA), one of the most advanced surgical robots, has been used in 1.5 million laparoscopic surgical operations globally over the past decade [19]. Nevertheless, although the development of the surgical methods has brought numerous advantages, it still needs for more than one surgeon to perform robotic surgery, as shown in Fig. 1.3. Due to this reason, as it can be shown in the figure, current operation room for robotic surgery is too messy and therefore still needs improvement. To resolve this issue, Hands-On-Throttle-And-Stick (HOTAS) controller is adopted to current master interface of laparoscopic surgical robot system, as shown in Fig. 1.4. HOTAS is used for flight control in the aerospace field and it can control hundreds of functions and provide feedback to the pilot about flight conditions. In this sense, the number of pilots inside the cockpit was reduced from two to one with the advent of HOTAS controller. Similarly, it can be used to help surgeons perform additional surgical operations and thereby overcome current situation of operation room.

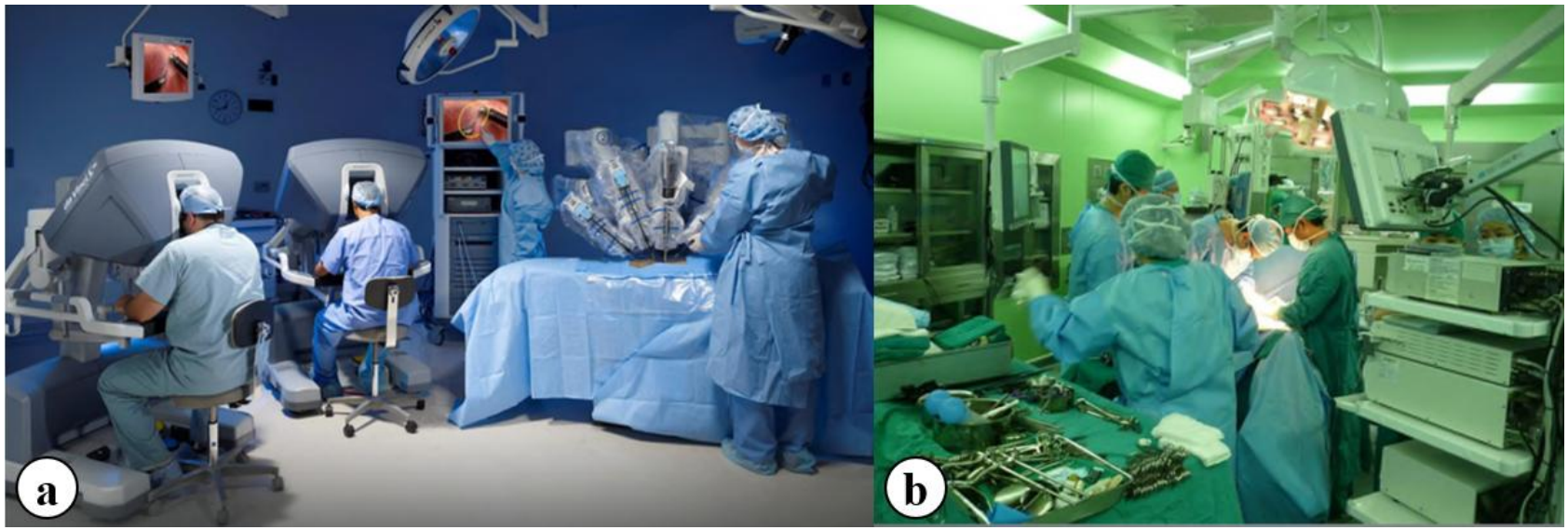

Fig. 1.3 (a) Robotic surgery performed by more than one surgeon [23]. (b) Actual operation room environment [24].

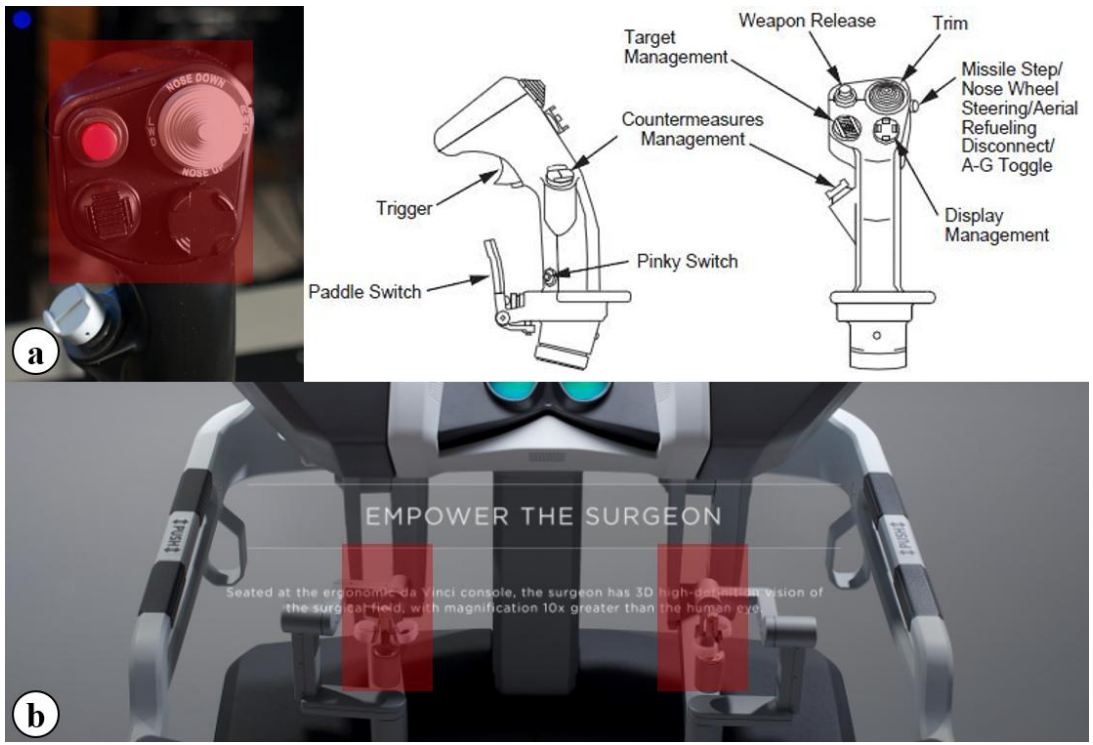

Fig. 1.4 (a) Hands-On-Throttle-And-Stick (HOTAS) used for flight control in the aerospace field [25]. (b) Target position for installing additional master interfaces in current laparoscopic surgical robot system [26].

For this purpose, two types of additional master interfaces are proposed in this research. More specifically, proposed additional master interfaces can be installed on current da Vinci laparoscopic surgical robot system and easily manipulated by surgeon's index finger which is currently only used for operating the finger clutch button. In addition, two application systems are proposed in this research to enhance function of laparoscopic surgical robot system based on below clinical needs.

Firstly, a robotic assistant is proposed for surgeon to additionally perform assistant's role in robotic surgery, such as resected object or foreign object removal, which was originally performed by surgeon in non-robotic laparoscopic surgery or laparotomy. This solution is not only able to decrease surgeon fatigue and operation time by eliminating communication process with assistants, and also able to resolve collision between the operation robot arms and the assistant instrument that can be caused by an inexperienced assistant or miscommunication and misaligned intent between the surgeon and the assistant [27-38], which can cause injury to patients [11, 19, 39-41]. Several solutions have been proposed. For example, a manipulator with a relatively small mass, which reduces the collision force, and force-feedback system has been proposed [40]. A surgery simulator for real-time collision processing and visualization that is able to prevent several types of collisions has also been developed [42]. A novel surgical robot design that minimizes the operating envelope during surgery has also been proposed [43]. In the

proposed design, the operating envelope is minimized to help the assistant to work alongside the robot, and also results in fewer collisions during surgery. A fourth arm that the operating surgeon can utilize for key steps and maneuvering during operations has also been proposed for the da Vinci surgical robot system [44]. This system reduce operation time and avoids collisions between the operating robot arm and the assistant's instrument by turning over control of the assistant's instrument to the surgeon, just as the proposed system.

Secondly, a stereo endoscope system that can be controlled by proposed additional master interfaces is proposed to overcome current control techniques needed for manipulating the endoscope system. In this scenario, the surgeon has to abandon the control of the patient side manipulator (PSM) by using a clutch button or pedal in order to control the endoscope system to change his/her view. The same control technique is required to regain control of the PSM [45]. This maneuver can lead to problems such as increased operation time, collision between surgical instruments, injury to patients (from surgical instruments being out of sight), and having to endure an unsatisfactory view to avoid swapping control [46]. Various approaches that attempt to solve this discontinuity issue proposed new master interfaces to control the endoscope system in parallel with the PSM. For example, a novel human-machine interface that tracks the surgeon's facial motion via his/her iris and a tracker placed on his/her forehead has been proposed to control the

position of the laparoscope [47]. A command interface for a combination of mouth gesture and voice command has also been proposed to control 3-DOF robotic endoscope systems [45]. An eye tracking endoscope control method has also been presented [48, 49] and a voice controlled robotic endoscope holder was developed [49]. Further, an interface that utilizes a pressure sensor sheet to track foot movement has been used to control surgical robot tools [50].

1.2.1. Additional Master Interfaces

To improve the utility of the current laparoscopic surgical robot system, additional master interfaces that can be installed on master interface of da Vinci surgical robot system have been proposed.

Firstly, a novel master interface (NMI), a wireless communication interface, was developed. The NMI is based on the HOTAS controller, which is widely used in aerospace for flight control [2]. The concept of HOTAS controller has been reported in our previous study [2, 51]. In this study, a multi-way switch and a wireless microprocessor were used to reflect the surgeon's decision. Further, the NMI developed is relatively small and can easily be attached to the master interface of da Vinci surgical robot system for easy access when the surgeon is manipulating the master interface. In this sense, the NMI can be regarded as a 9-way compact HOTAS. The performance test, latency, and power consumption of the developed NMI were verified by repeated experiments.

Secondly, the improved novel master interface (iNMI) is proposed which is an improved version of the NMI. The iNMI is also based on the HOTAS controller used broadly in flight control, and which was previously presented [2, 51]. In this study, a capacitive touch sensor array was developed and a

wireless microprocessor used to intuitively reflect the surgeon's decision. In addition, the size of the iNMI is small enough to be easily installed to the master interface of da Vinci surgical robot system to maximize convenience to the surgeon when using the iNMIs to manipulate the application systems with the MTMs. Thus, the iNMI is a capacitive touch type compact HOTAS. Multiple experiments were performed to evaluate the iNMI performance in terms of performance test, latency, and power consumption.

1.2.2. Application Systems

Although above-mentioned systems have been proposed partially based on the issue of increased operation time and collision between the operating robot arm and the assistant's instrument, they have several deficiencies: (i) they are limited to simulation and cannot be directly applied to the surgical robot system [42], (ii) they can only minimize or reduce, not prevent, collisions [40, 43], and (iii) the surgeon cannot simultaneously manipulate both the robotic assistant and the operation robot arm, resulting in discontinuous surgical operation [44]. In addition, this robotic assistant cannot perform surgical operations such as removal of resected tissue because it cannot move outside the incision.

This research proposes a robotic assistant that overcomes these issues. The system, which consists of an assistant robot arm and its wireless controller, aims to remove the cause of the increased operation time and collisions due to tiredness or miscommunication and misaligned intent between the surgeon and the assistant by allowing the surgeon to control the assistant instrument. Further, a wireless controller is used for simultaneous control of the operating robot arm and the robotic assistant, thereby preventing discontinuous surgical operation which is also the cause of the increased operation time. The robotic assistant consists of a 6-DOFs external robot arm and a surgical instrument developed based on the surgical-operation-by-wire (SOBW) concept that has been reported in our previous study [2, 51]. SOBW was inspired by the fly-by-wire (FBW) system in aerospace engineering, in which the wing control is based on electrical wires for reliable control [52], instead of a mechanical wires [53-56]. The concept is applied in the medical field with the mechanical strings in the surgical robot system replaced with electrical wires. In this sense, all the motions of the proposed robotic assistant, including the external robot arm and the surgical instrument, are actuated by electrical actuators such as alternating current servo motors and micromotor. Further, the yawing and pitching motions are removed from the surgical instrument as they are not necessary for the performance of dexterous movements. In exchange, the diameter of the proposed surgical instrument is 6 mm. This is smaller than that of the most extensively used da Vinci surgical robot system's 8 mm EndoWrist. The rolling, translational, and fulcrum point motions of the

surgical instrument are performed by the 6-DOFs external robot arm. The gripping motion is achieved by converting the rotational motion of the micromotor into translational motion using male and female screws, with the female screw linked to the gripper. Consequently, the gripping force can be controlled by adjusting the position of the micromotor. The durability of the surgical instrument developed was verified via a 1000 times of repeated durability tests. A da Vinci research kit (dVRK), donated by Intuitive Surgical, Inc., was used in this study to perform as the operation robot arm system. The dVRK is a research kit consisting of several parts, including master tool manipulators (MTMs), PSMs, stereo viewer, and foot pedal, from the first generation da Vinci surgical robot system.

Simple peg tasks using the robotic assistant were also performed to evaluate the clinical applicability of the proposed robotic assistant. In addition, an *in vitro* test of semi-automatic resected object removal was conducted using the proposed robotic assistant and the dVRK system to examine the performance of the proposed system. The results indicate that this novel surgical robot system can be effectively utilized for laparoscopic robotic surgery.

In addition, although the previously proposed interfaces allow simultaneous control of the endoscope system and the PSMs, they also have limitations: i) they cannot be adapted to current robot-assisted surgical systems as the surgeon's head and foot are already occupied [47, 50], ii) they prevent surgeons from giving verbal orders, which is essential during surgical

operations, as they use mouth and voice for control [44, 49], and iii) they are prone to erroneous and unintended endoscopic movements that can in turn result in greater harm to patients [49, 57].

In this study, a stereo endoscope system that can be controlled by the proposed additional master interfaces is also proposed to overcome these limitations with the objective of reducing operation time and surgeon fatigue as a result of enabling continuous surgical operation by allowing simultaneous control of the PSMs and the endoscope system. The system consists of a dVRK, a 4-DOFs endoscope control system (ECS), a simple three-dimensional (3D) endoscope, and its additional master interfaces. The dVRK is used as operation robot system, which is a research kit donated by Intuitive Surgical, Inc., and includes MTMs, PSMs, a foot pedal, and a stereo viewer from the first generation of the da Vinci surgical robot system. Since the endoscope system of da Vinci surgical robot is not included in the dVRK system, the 4-DOFs endoscope system and the simple 3D endoscope are developed to provide stereo view to the surgeon. The 4-DOFs ECS, developed based on SOBW concept to control the position of the endoscope, consists of four servo motors, which facilitate pitching, yawing, rolling, and translational motions, and a two-parallel link structure that enables stable fulcrum point motion essential for laparoscopic surgery. The simple 3D endoscope consists of two complementary metal-oxide-semiconductor (CMOS) camera modules that provide real-time stereo view to the surgeon via the stereo viewer of the

dVRK. The original images obtained by the sensors undergo a stereo calibration and a stereo rectification process that results in stereo vision. The outer diameter of the developed endoscope is 10 mm and each CMOS module is capable of generating images with a resolution of 640 × 480 pixels. The additional interfaces are used to enable simultaneous control of the PSMs and the endoscope system in order to eliminate the possibility of surgical instruments being out of sight and therefore prevents collision between surgical instruments and injury to patients. Furthermore, this will also result in reduced surgical operation time and, consequently, surgeon fatigue. Modified peg transfer tasks which require adjustment of field of view throughout the tasks were also carried out to evaluate its clinical applicability and ease of use. The results indicate that this novel surgical robot system can be effectively utilized for laparoscopic robotic surgery.

2. Materials and Methods

2.1. Additional Master Interfaces

2.1.1. Novel Master Interface: 9-way Compact Hands-On-Throttle-And-Stick

The NMI—a wireless communication interface—was developed to carry out the surgeon's intent as regards control of the proposed application systems. The NMI was designed based on HOTAS, using a multi-way switch (RKJXL100401 V, ALPS, Tokyo, Japan)—more specifically, it has eight ways with a center push—for the surgeon to manipulate. In addition to the multi-way switch, the NMI comprises one Li-MnO2 type Lithium button cell battery (CR2032, Panasonic, Osaka, Japan), one 10- to 4-line encoder (CD40147B, Texas Instruments, Dallas, TX, USA), one Arduino-based microprocessor with a Bluetooth low energy radio frequency module (RFD 22301, RFduino, Hermosa Beach, CA, USA), and several resistors and

capacitors to constitute the circuit. The circuit was designed using Altium Designer (Altium, San Diego, California, United States). As it can be shown in Fig. 2.1, the NMI consists of 4 layer. The first layer contains the multi-way switch and microprocessor in order to allow surgeon to easily manipulate the multi-way switch and prevent communication noise caused by covering the microprocessor using metal parts of the MTMs of dVRK. The fourth layer consists of other parts of the NMI, such as the encoder, battery shield, and etc. The second the third layer serve as ground and power layer to the NMI. The multi-way switch has relatively small operating force in order to be easily controlled by the surgeon with comfort [58], and the output signal for each way of the multi-way switch is encoded as a four-digit number, representing a possible decision by the surgeon, via the 10- to 4-line encoder. On entering the Bluetooth module the four-digit number is sent to the wireless data receiver, where it is recognized as a command by the controller that manipulates the surgical instrument and the external robot arm based on the received signal. A circuit for this purpose was designed and implemented on a printed circuit board, and then assembled with other parts, as shown in Fig. 2.2-(a). To manipulate the NMIs simultaneously with MTMs, the two NMIs are tightly attached to two MTMs of the dVRK system using a special holder as shown in Fig. 2.2-(b). The reason for this is to not interrupt the operation of finger clutch of MTM which exists from the da Vinci Si system [59], and allow the surgeon to control the NMI using the index finger which is not used for manipulating the MTM, except for operating the finger clutch, as shown in

Fig. 2.2-(c). Each NMI has dimensions 33 × 35 mm to ensure that they do not disrupt the motion of the MTMs. Fig. 2.3 shows the mapping information between the NMI and the surgical instrument. NMI attached to the left MTM manipulates the fulcrum point motion, whereas that attached to the right MTM operates the translational and rolling motions. The gripping motion can be controlled by the center push of both left and right NMI. Thus, the translational, fulcrum point, and rolling motions, in addition to the gripping motion of the robotic assistant can be simultaneously controlled with PSMs by manipulating the two NMIs and MTMs.

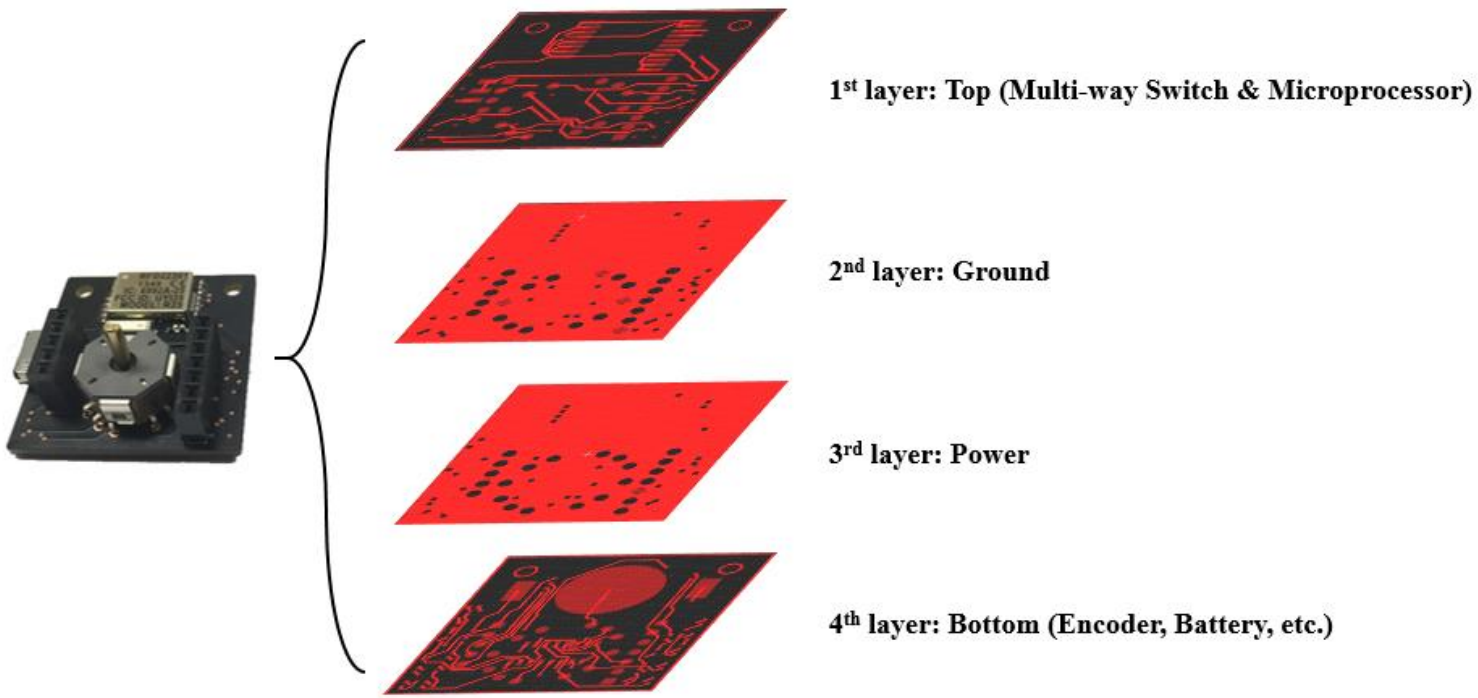

Fig. 2.1 Layer information of proposed novel master interface (NMI).

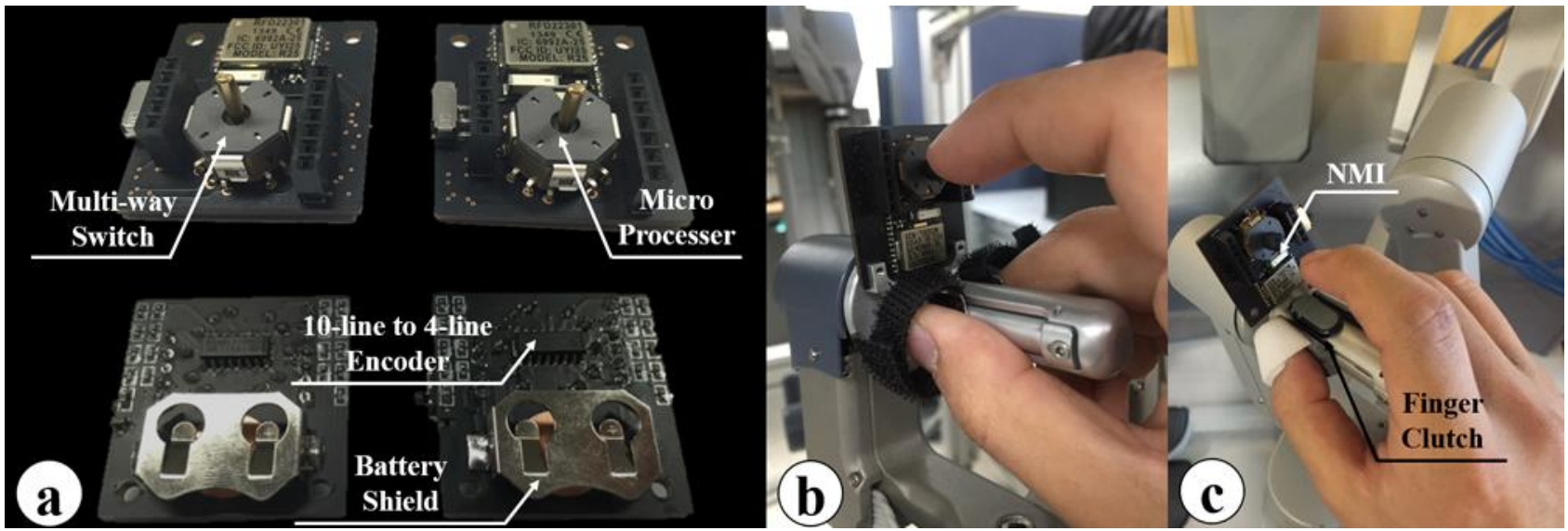

Fig. 2.2 Developed NMI. (a) Front and back side of the NMI. (b) The NMI attached on the MTM of the dVRK system using the special holder. (c) Usage of the index finger to operate finger clutch and the NMI.

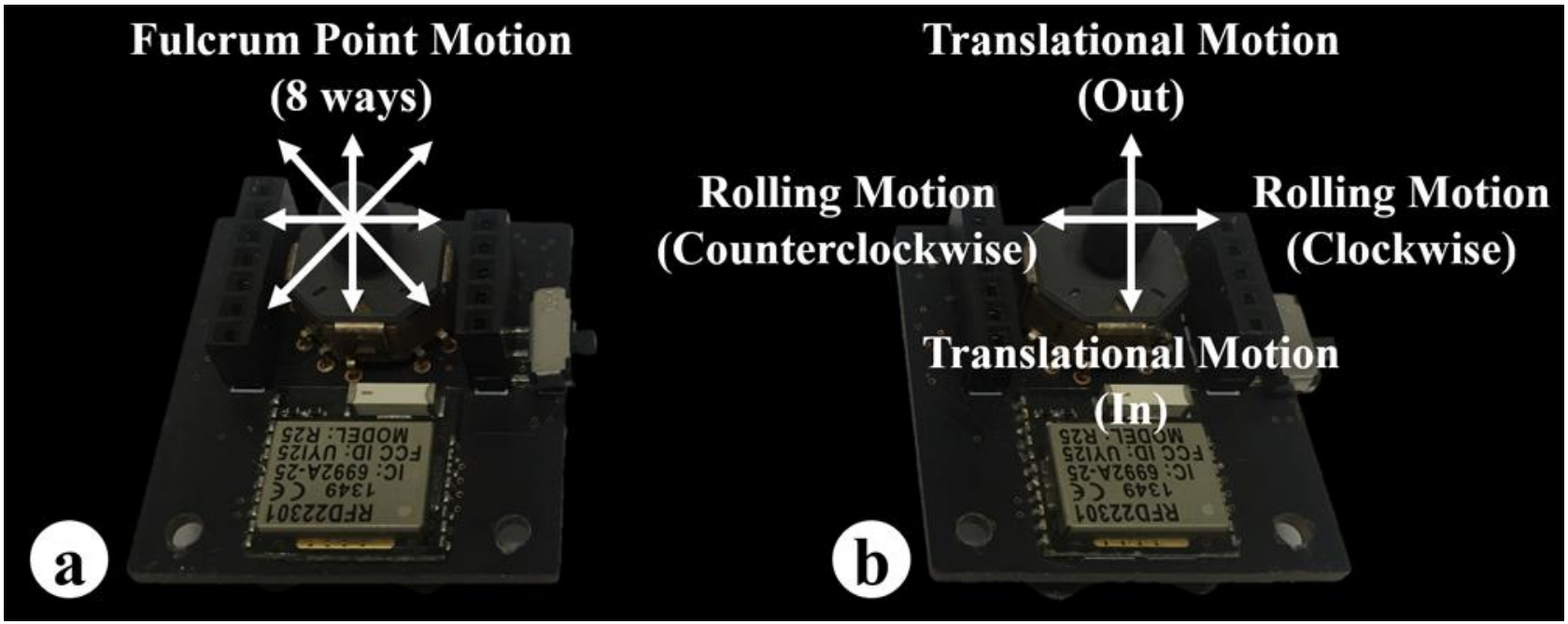

Fig. 2.3 Mapping information between the NMI and the surgical instrument. (a) Left NMI. (b) Right NMI.

2.1.2. improved Novel Master Interface: Capacitive Touch Type Compact Hands-On-Throttle-And-Stick

The iNMI, which is a wireless communication interface, was developed to intuitively reflect the surgeon's decision as regards control of the application systems. The iNMI was also designed based on the HOTAS concept [2, 60]. To more intuitively reflect the surgeon's intent, the iNMI utilizes a capacitive touch sensor array, based on a resistor-capacitor (RC) circuit with the capacitor as the touch sensor [61], instead of a multi-way switch. When the user touches the touch sensor, the RC time constant increases as the human body can be regarded as a relatively large capacitor [62]. Further, as the RC time constant can be calculated by setting a new state to the input of the RC circuit and then waiting for the output to be changed to the same state as the input, the touch status of the touch sensor can be determined. The gesture information generated from using the iNMI is obtained via the touch sensors array placed on the front of the iNMI, which comprises 25 capacitive touch sensors, as shown in Fig. 2.4-(a). The size of the each touch sensor was decided based on previous research for contact region of finger touch [63]. In this sense, one element of the capacitive touch sensors array has a shape of circle with a diameter of 4 mm. Then, the sensors were aligned with equidistant intervals considering the overall dimension of the iNMI, which is

33 mm × 35 mm to ensure that they do not disrupt the motion of the MTMs, as shown in Fig. 2.5. The circuit was designed using Altium Designer (Altium, San Diego, California, United States). The iNMI also consists of 4 layer as it can be shown in Fig. 2.6. Similarly, the second the third layer serve as ground and power layer to the iNMI, respectively. The first layer only contains the capacitive touch sensors array in order to prevent malfunction of the iNMI since the iNMI is highly sensitive to value of capacitor connected to each capacitive touch sensor. The fourth layer consists of other parts of the iNMI, such as the microprocessor, battery shield, and etc.

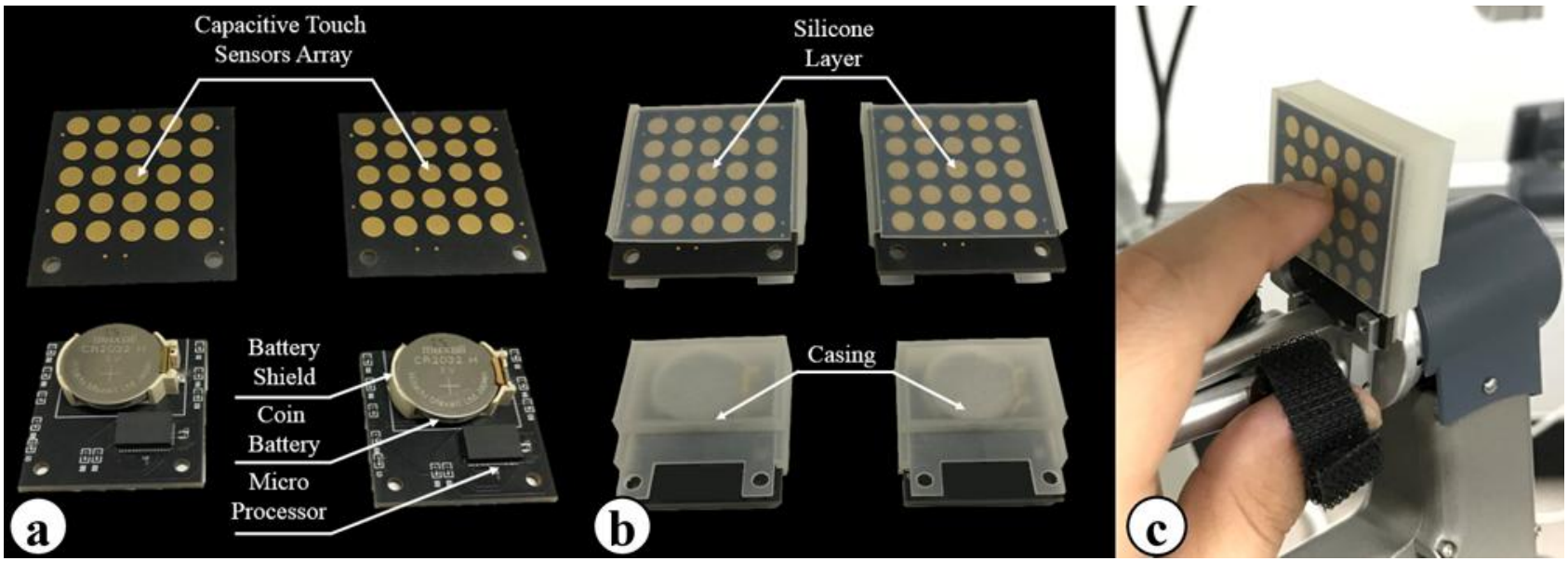

Fig. 2.4 Developed improved novel master interface (iNMI). (a) Front and back sides of the iNMI. (b) Case and silicone top layer to protect the iNMI. (c) The iNMI attached on the MTM of the dVRK system using the special holder.

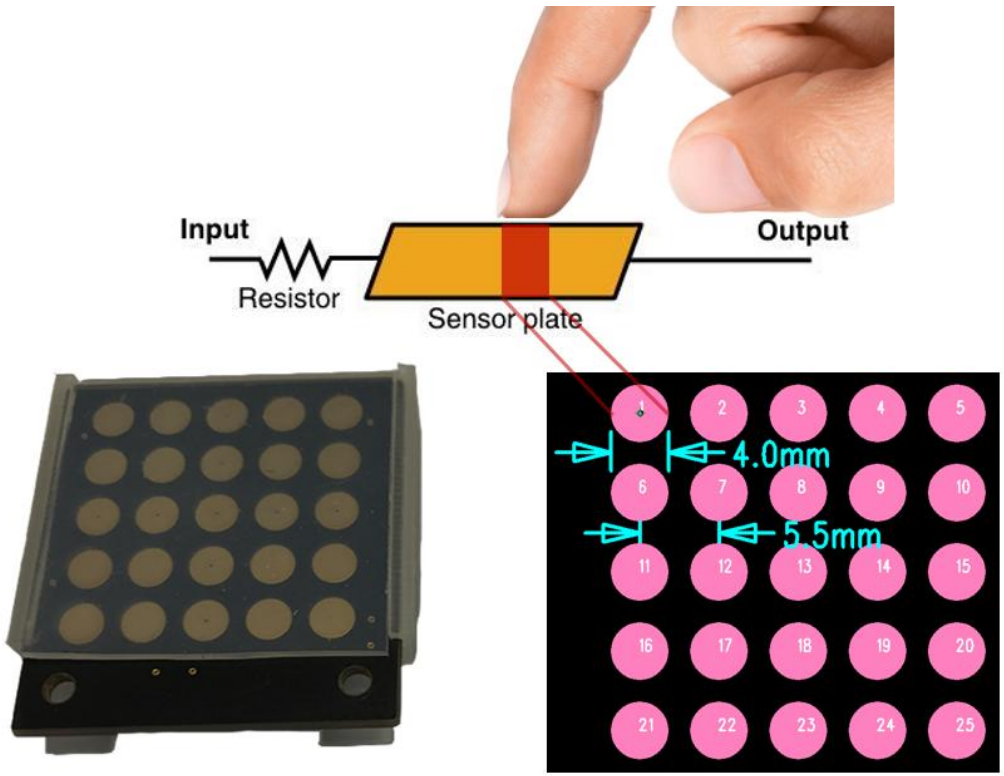

Fig. 2.5 Design of proposed touch sensors array.

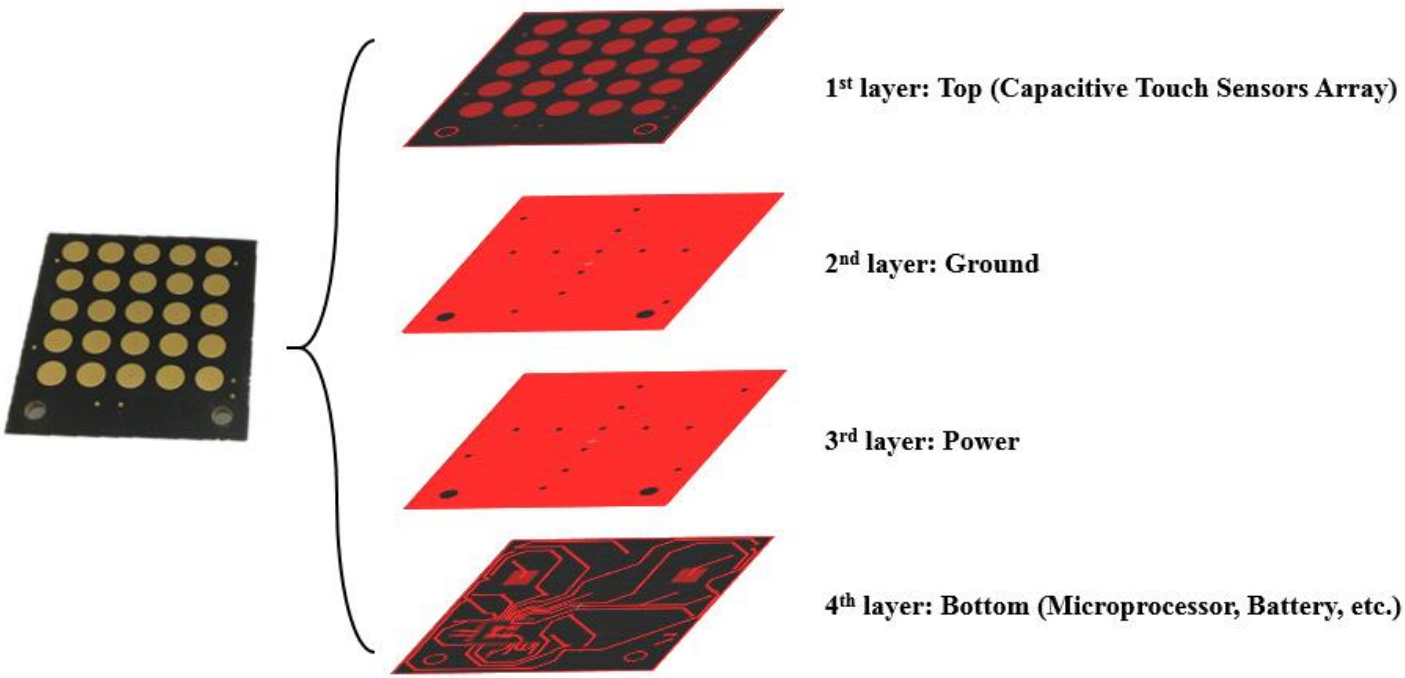

Fig. 2.6 Layer information of the iNMI.

The intent of the surgeon is determined from the touch status of the capacitive touch sensors array. In addition to the capacitive touch sensors array, the iNMI comprises one Arduino-based microprocessor with a Bluetooth low energy radio frequency module (RFD 77101, RFduino, Hermosa Beach, CA, USA), one Li-MnO2 type Lithium button cell battery (CR2032, Panasonic, Osaka, Japan), and several resistors and capacitors to complete the circuit.

Each capacitive touch sensor is connected to the microprocessor to receive the RC time constant for perceiving the touch status of the capacitive touch sensor. To interpret the received touch information of the touch sensor array, a specific Arduino algorithm was developed to detect gesture information generated by the surgeon, such as upward swipe, downward swipe, forward swipe, and backward swipe. Once the gesture information is created, the Bluetooth module sends the information to the wireless data receiver, and the received signal is recognized as a command by the controller to manipulate the application systems. To achieve above functions, a circuit was designed and a printed circuit board including the capacitive sensor array was consequently manufactured. Several parts were used for the board as shown in Fig. 2.4-(a). Further, it allows the surgeon to control the iNMI using the index finger that is not used to manipulate the MTM, but only to operate the finger clutch. Furthermore, in order to protect the iNMI's circuit and the capacitive touch sensor array, a customized outer case was designed and manufactured. The touch sensor array is covered with a silicone layer, as shown in Fig. 2.4-(b). To manipulate the iNMIs simultaneously with the MTMs, the two iNMIs

are tightly installed to the two MTMs of the dVRK system using a customized holder, as shown in Fig. 2.4-(c). In this way, the operation of the finger clutching the MTM is not interrupted, as occurs when using the da Vinci Si system [59]. Fig. 2.7 shows the mapping information of the iNMI. As can be seen in the figure, the pitching motion and the yawing motion can be controlled by one of the two iNMIs, whereas the rolling motion and the translational motion can only be achieved by a combination of gestures generated by the iNMIs attached on the left and right MTMs. The mapped motions were deliberately designed to be similar to common touch gestures carried out in daily living activities using two fingers to ensure intuitive control by the surgeon. Thus, the pitching, yawing, rolling, and translation motions of the application systems can be simultaneously controlled with PSMs by manipulating the two iNMIs and MTMs.

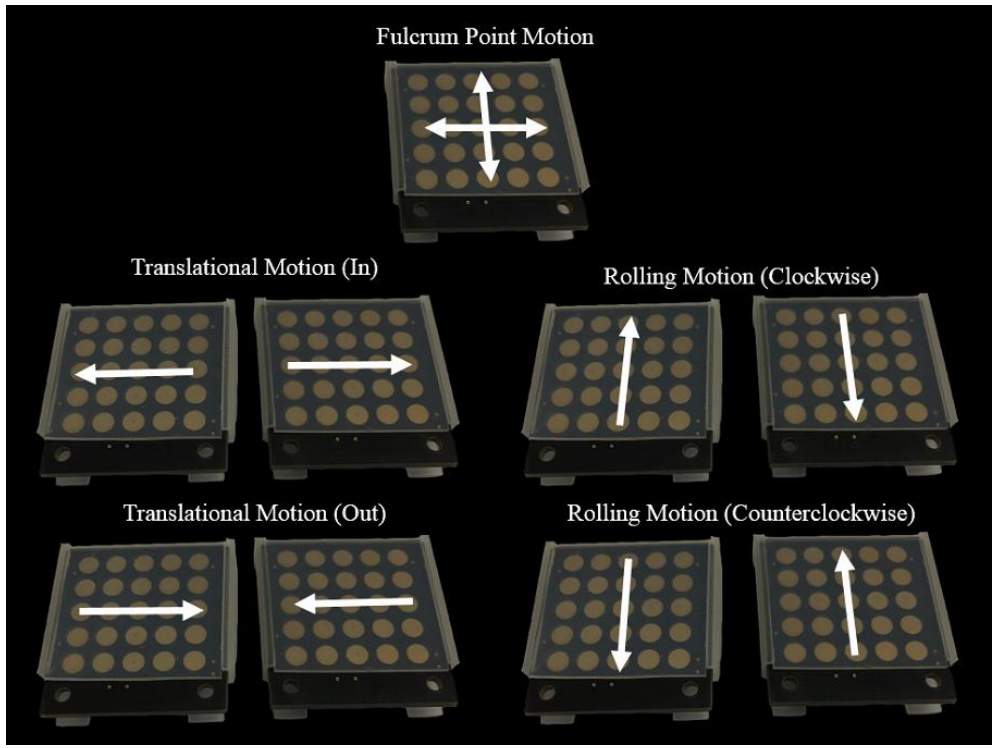

Fig. 2.7 Mapping information of the iNMI. The fulcrum point motion can be achieved using one of the two iNMIs while the translational motion and rolling motion can only be performed by combination of two iNMIs' gesture input.

2.2. Application Systems

2.2.1. Robotic Assistant

Overview

The robotic assistant developed to overcome the limitations stated above comprises four parts: (i) dVRK system to perform as the operation robot, (ii) surgical instrument with the diameter of 6 mm, (iii) 6-axis external robot arm that provides translational, fulcrum point, and rolling motions, and (iv) two additional master interfaces that respectively reflect the surgeon's decision to control the external robot arm and the surgical instrument.

These parts, with the exception of the dVRK system, were integrated via the LabVIEW® and the PXIe controller (LabVIEW® 2013, PXIe-8135 and 1062Q, National Instruments, Austin, TX, USA, Used valid license). The control flow of the overall system is illustrated in Fig. 2.8. As shown in the figure, the surgeon can simultaneously control both PSMs—the operation robot arms and the robotic assistant developed—by manipulating the two MTMs and the two additional master interfaces. Continuous surgical operation can thus be ensured via this control flow. The gripping motion of the surgical instrument is facilitated using an electronically commutated micromotor with the diameter of 4 mm (EC-4 motor, EPOS2 controller,

Maxon Motor, Brünigstrasse, Sachseln, Switzerland), which is able to rotate in both clockwise and counterclockwise direction.

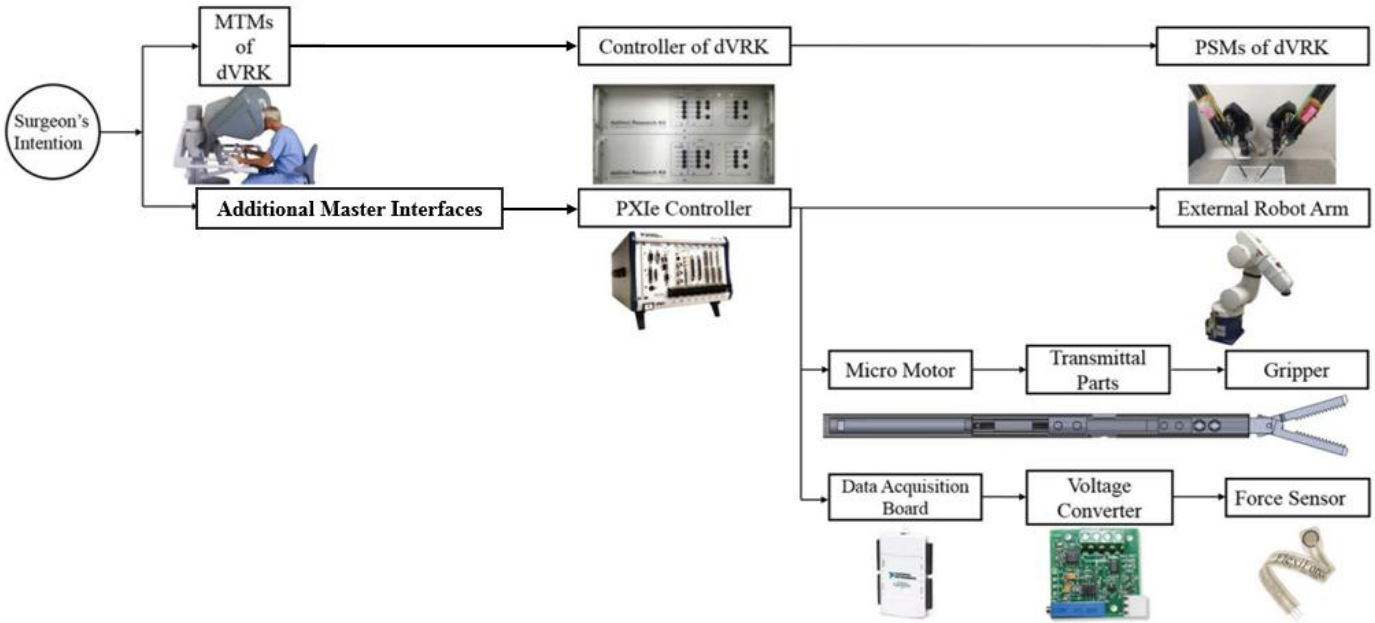

Fig. 2.8 Control flow of the proposed robotic assistant driven by the surgeon's intention. Software integration is based on the LabVIEW® software.

da Vinci research Kit (dVRK)

The dVRK system was used to perform as an operation surgical robot system. The dVRK system comprises one foot pedal, two MTMs, two PSMs, and one stereo viewer to provide a three-dimensional stereo view for the user, as shown in Fig. 2.9. Two webcams are installed to provide images. Each MTM is able to manipulate its respective PSM during laparoscopic surgery. The dVRK system was integrated with the robotic assistant.

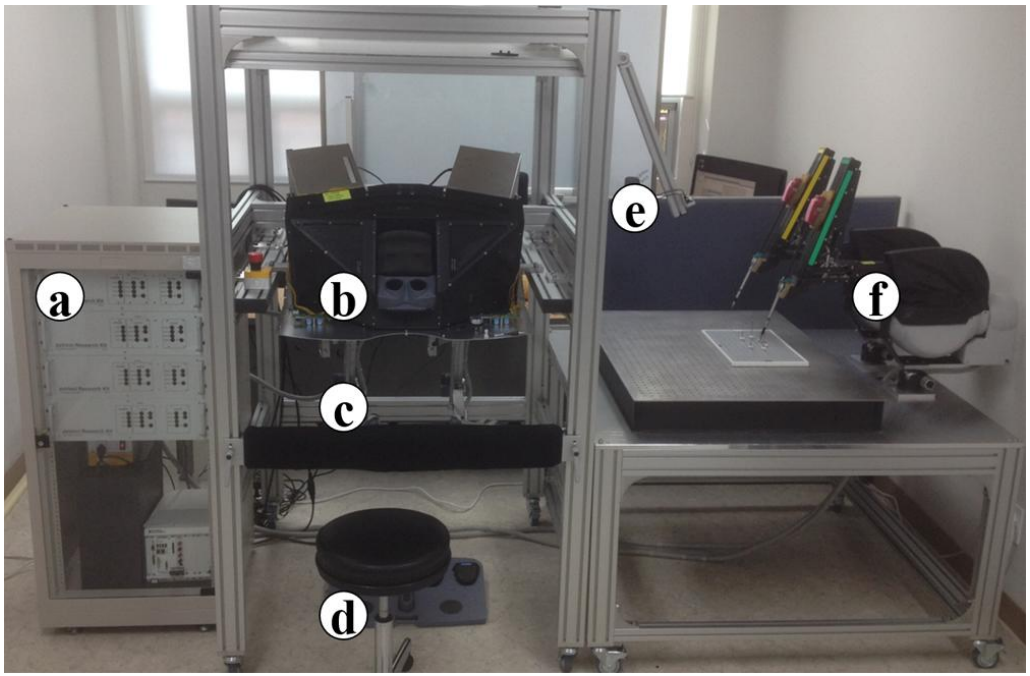

Fig. 2.9 Overall system of the da Vinci research kit (dVRK). (a) Controllers. (b) Stereo viewer. (c) Master tool manipulators (MTMs). (d) Foot pedal. (e) Two webcams for providing images. (f) Patient side manipulators (PSMs). dVRK is used as operation surgical robot system in this research.

Surgical Instrument

A surgical instrument, which can perform only gripping motion, was developed specifically for the laparoscopic surgical robot system. Yawing and pitching motions were removed as they are not necessary for the assistant surgical instrument to perform dexterous motion. In exchange, the diameter of the proposed surgical instrument is 6 mm. This is smaller than that of the most extensively used da Vinci surgical robot system's 8 mm EndoWrist and comparable with that of the 6 mm EndoWrist which has less applications. The rolling motion of the surgical instrument is achieved by the external robot arm by installing the instrument as an end-effector. Unlike other systems [7, 64], the surgical instrument can be easily replaced during surgery. The actuating force of the surgical instrument's gripping motion is generated by converting the rotation of the micromotor's shaft into translational motion using a male and female screw arrangement similar to the ball screw mechanism. Actuation of the micromotor causes the male screw to rotate around a fixed axis and the female screw to consequently move translationally along a straight line guided by the outer shell. Linear motion of the linkage is enabled by linking the female screw with the linkage. Further, the gripping motion is then generated by linking the linkage and the gripper, which was cut off from a laparoscopic forceps (Laparoscopic forceps, Ethicon Endo-Surgery, Cincinnati, Ohio, USA) and modified by adding a hole for the connection. This was possible because each side of the gripper is based on the slider crank mechanism, which can convert linear motion to rotational motion as a reciprocating pump engine.

Each side of the gripper is aligned symmetrically with respect to the longitudinal axis, and thus can be actuated by the linear motion of the linkage simultaneously. Therefore, open and close motion of the gripper are then achieved by clockwise and counterclockwise rotation of the micromotor's shaft. The overall design and the actual image of the surgical instrument are illustrated in Figs. 2.10 and 2.11. The outer shells and the other parts of the surgical instruments, such as the male and female screws, and the linkage were manufactured using aluminum and assembled with the micromotor and the gripper, as shown in Fig. 2.11. The surgical instrument was designed to be 300 mm long for surgical usability.

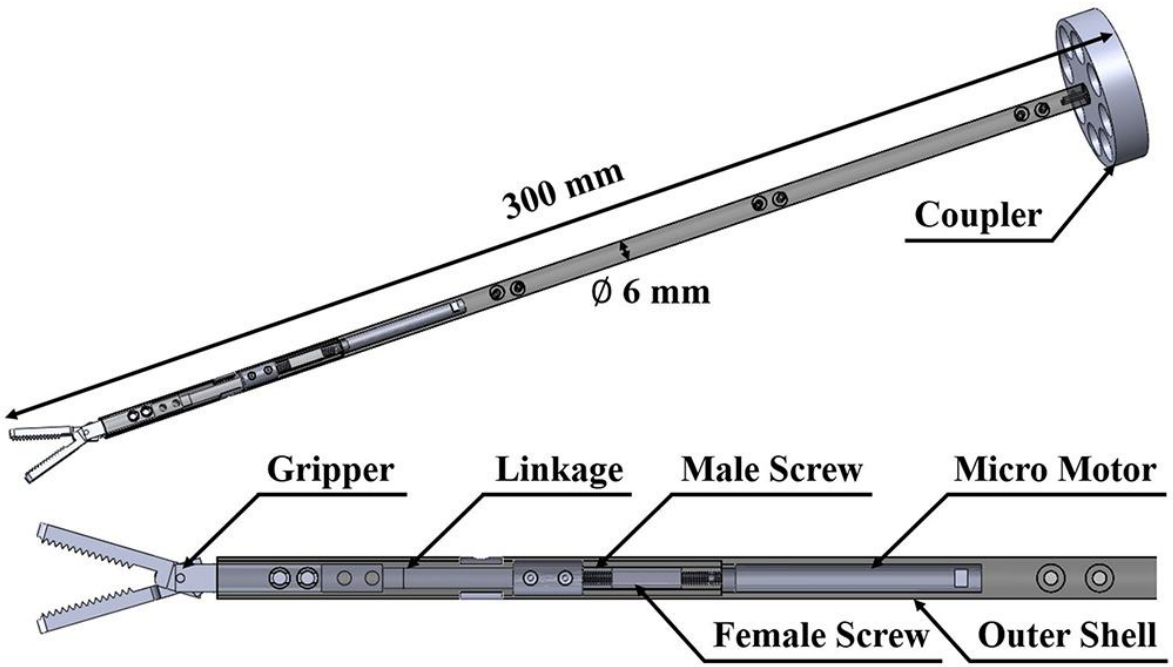

Fig. 2.10 Design of the proposed surgical instrument. The gripping motion is achieved by converting the micro motor's rotation motion into linear motion by male and female screw and linking the gripper with the female screw through the linkage. The length and the diameter of the surgical instrument is designed as 300 mm and 6 mm, respectively.

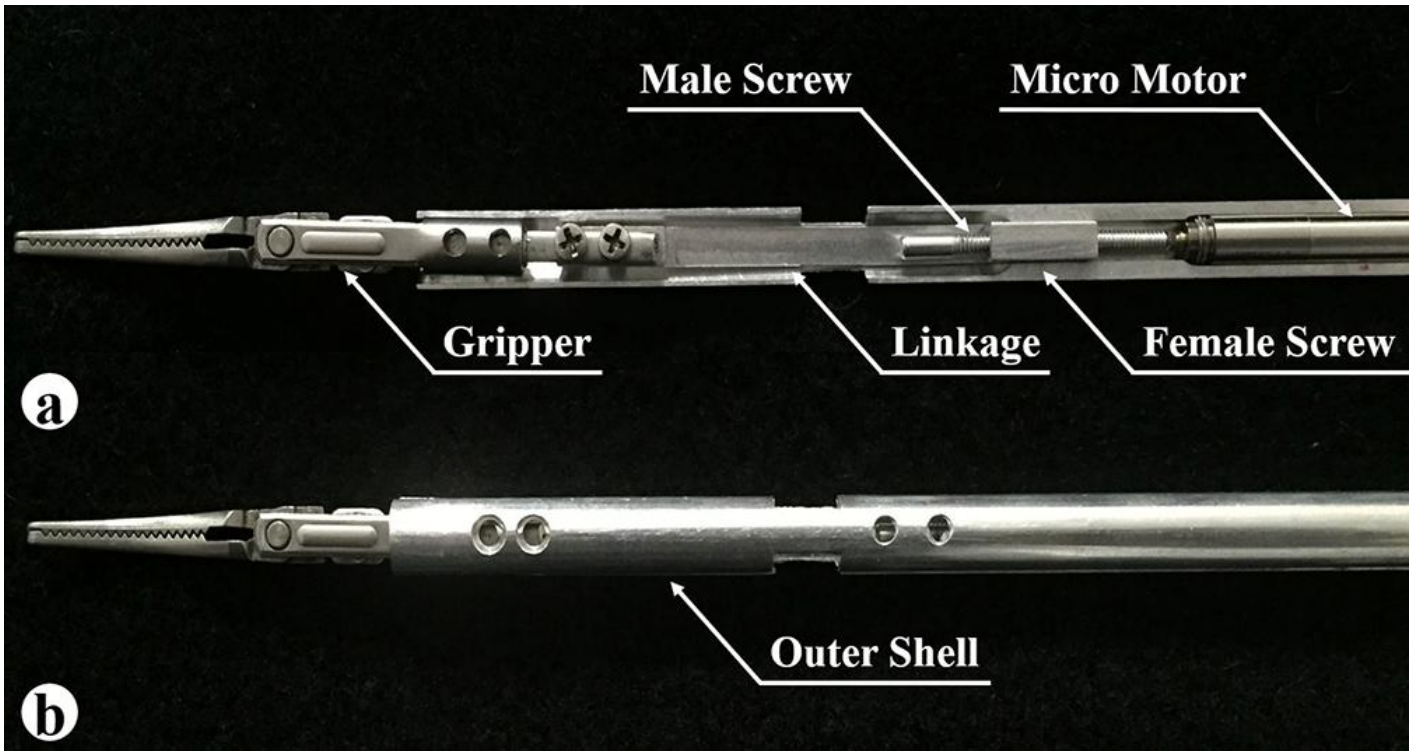

Fig. 2.11 Surgical instrument manufactured using aluminum. (a) The surgical instrument without the upper outer shell. Actual position of the micro motor, male and female screw, linkage, and the gripper is shown. (b) The surgical instrument with the upper outer shell.

External Robot Arm

An external robot arm (VS-6556G, DENSO, Kariya, Aichi Prefecture, Japan) with six joints, from *J1* to *J6*, is used to perform the surgical instrument's translational, fulcrum point, and rolling motions, as shown in Fig. 2.12. The translational and the fulcrum point motions are achieved by coordinating joints *J1* to *J5* and controlling them based on the tool coordinates system, which sets the origin of the external robot arm to the origin of the end-effector. To perform the fulcrum point motion, a virtual remote center of motion (RCM) algorithm was applied to the external robot arm since it did not employ a RCM mechanism as the PSM of the dVRK system did. Thus, the RCM point of the external robot arm can be adjusted by the virtual RCM algorithm. As for the rolling motion, unlike the da Vinci surgical robot system's Endowrist which can perform rolling motion by itself [65], it is achieved by joint *J6* of the external robot arm. The forward kinematics of the external robot arm has been described in previous work [2].

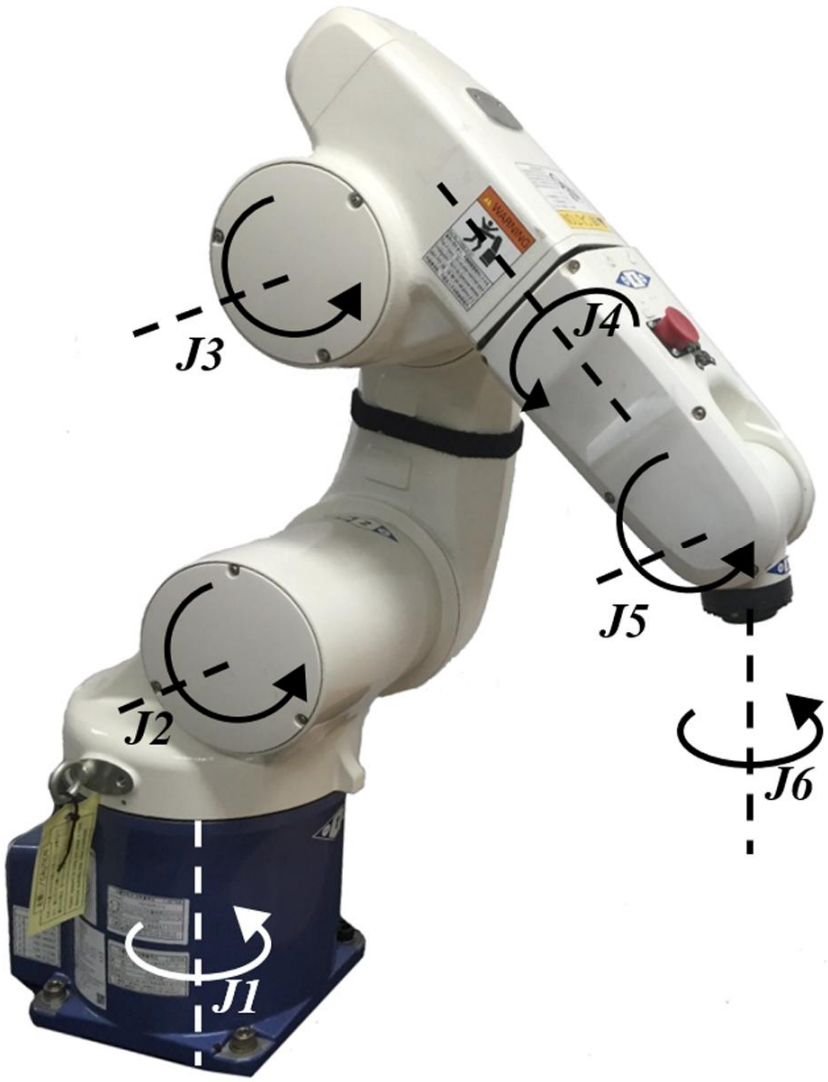

Fig. 2.12 Joint information of the 6-degrees of freedom (DOFs) external robot arm. The fulcrum point motion and the translational motion of the surgical instrument are achieved by complex combination from *J1* to *J5*. The surgical instrument's rolling motion is achieved by *J6*.

Forward Kinematics of the System

Fig. 2.13 shows the kinematic structure of the entire system, except for the gripping motion. *J1-J6* represent the external arm parts. Table 2.1 shows the Denavit-Hartenberg (D-H) parameters of this system.

Table 2.1 Forward kinematics of the system (D-H parameters)

Joint	α_{i-1} (rad)	a_{i-1} (mm)	d_i (mm)	θ_i (rad)
1	0	0	335	θ_1
2	$-\frac{\pi}{2}$	75	0	$\theta_2 - \frac{\pi}{2}$
3	0	270	0	θ_3
4	$-\frac{\pi}{2}$	90	295	θ_4
5	$\frac{\pi}{2}$	0	0	θ_5
6	$-\frac{\pi}{2}$	0	296	$\theta_6 + \frac{\pi}{2}$

Forward kinematics and D-H parameters of the system are defined by Fig. 2.13 and Table 2.1. The external arm and surgical instrument are executed using several control algorithms.

With reference to Table 2.1, each joint's information such as operational angle and other information could be confirmed. These homogeneous

transformation matrices are inferred from D-H convention theory [66]. From these parameters, equation (2.1), and Fig. 2.13, the homogeneous transformation matrices of the proposed system's each joint could be obtained. According to equation (2.1), each joint is designated to unique homogeneous transformation matrix.

$$ {}^{i-1}_{i}T = \begin{bmatrix} cos(\theta_i) & -sin(\theta_i) & 0 & a_{i-1} \\ \sin(\theta_i)cos(\alpha_{i-1}) & \cos(\theta_i)\cos(\alpha_{i-1}) & -sin(\alpha_{i-1}) & -\sin(\alpha_{i-1})d_i \\ sin(\theta_i)\sin(\alpha_{i-1}) & cos(\theta_i)\sin(\alpha_{i-1}) & cos(\alpha_{i-1}) & cos(\alpha_{i-1})d_1 \\ 0 & 0 & 0 & 1 \end{bmatrix} \tag{2.1} $$

Each joint's information such as operational angle and other information could be confirmed. From these parameters, the homogeneous transformation matrices are given as equation (2.2)–(2.7).

$$ {}^{0}_{1}T = \begin{bmatrix} cos\theta_1 & -sin\theta_1 & 0 & 0 \\ sin\theta_1 & cos\theta_1 & 0 & 0 \\ 0 & 0 & 1 & d_1 \\ 0 & 0 & 0 & 1 \end{bmatrix} \tag{2.2} $$

$$ {}^{1}_{2}T = \begin{bmatrix} sin\theta_2 & cos\theta_2 & 0 & a_1 \\ -cos\theta_2 & sin\theta_2 & 0 & 0 \\ 0 & 0 & 1 & 0 \\ 0 & 0 & 0 & 1 \end{bmatrix} \tag{2.3} $$

$$ {}^{2}_{3}T = \begin{bmatrix} cos\theta_3 & -sin\theta_3 & 0 & a_2 \\ sin\theta_3 & cos\theta_3 & 0 & 0 \\ 0 & 0 & 1 & 0 \\ 0 & 0 & 0 & 1 \end{bmatrix} \quad (2.4) $$

$$ {}^{3}_{4}T = \begin{bmatrix} cos\theta_4 & -sin\theta_4 & 0 & a_3 \\ 0 & 0 & 1 & d_4 \\ -sin\theta_4 & -cos\theta_4 & 0 & 0 \\ 0 & 0 & 0 & 1 \end{bmatrix} \quad (2.5) $$

$$ {}^{4}_{5}T = \begin{bmatrix} cos\theta_5 & -sin\theta_5 & 0 & 0 \\ 0 & 0 & -1 & 0 \\ sin\theta_5 & cos\theta_5 & 0 & 0 \\ 0 & 0 & 0 & 1 \end{bmatrix} \quad (2.6) $$

$$ {}^{5}_{6}T = \begin{bmatrix} -sin\theta_6 & -cos\theta_6 & 0 & 0 \\ 0 & 0 & 1 & d_6 \\ -cos\theta_6 & sin\theta_6 & 0 & 0 \\ 0 & 0 & 0 & 1 \end{bmatrix} \quad (2.7) $$

The transformation matrices of the external arm is given by (2.8). Equation (2.8) describes the position and orientation of the external arm's translational and fulcrum point movements.

$$ {}^{0}_{6}T = {}^{0}_{1}T\,{}^{1}_{2}T\,{}^{2}_{3}T\,{}^{3}_{4}T\,{}^{4}_{5}T\,{}^{5}_{6}T \quad (2.8) $$

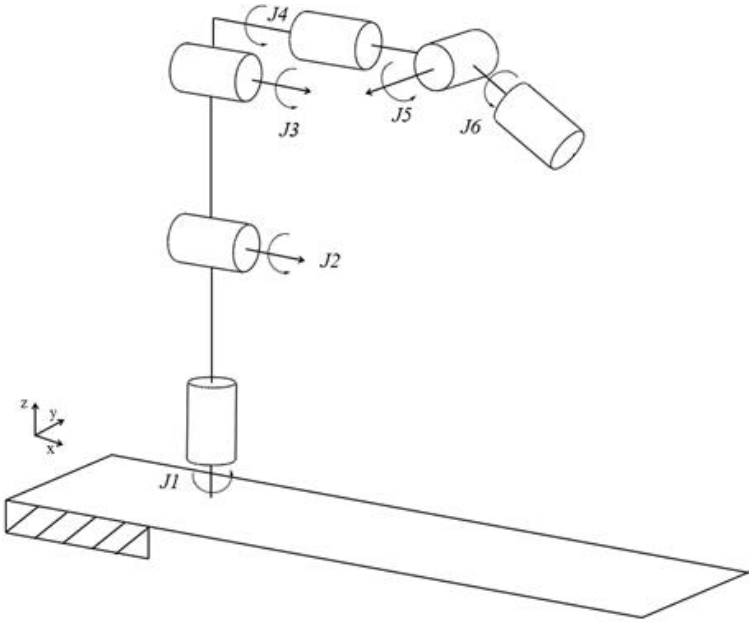

Fig. 2.13 Kinematic structure of the system.

2.2.2. Stereo Endoscope System

Overview

To overcome the above-mentioned limitations, a novel stereo endoscope system consisting of the following four parts was developed: i) a simple 3D endoscope that provides 3D vision to the surgeon via a stereo viewer, ii) a 4-DOFs ECS to control the position of the developed endoscope, iii) a dVRK-based operating robot system which provides 3D stereo view constructed using stereo calibrated and rectified images obtained from the developed stereo endoscope, and iv) two additional master interfaces for the surgeon to intuitively control both the 4-DOFs ECS and the PSM simultaneously.

The proposed system was integrated based on the PXIe controller and LabVIEW® (PXIe-8135 & 1062Q, LabVIEW® 2013, National Instruments, Austin, TX, USA), except for the dVRK system. Fig. 2.14 illustrates the integrated system's control flow. As illustrated in the figure, simultaneous operation of both PSMs and the developed 4-DOFs ECS is enabled via the two MTMs and the two additional master interfaces. Discontinuous surgical flow can then be overcame. The rolling motion, pitching motion, yawing motion, and translational motion of the 4-DOFs ECS are facilitated by four servo motors (Ezi-Servo Series, Fastech, Bucheon, South Korea) based on SOBW concept.

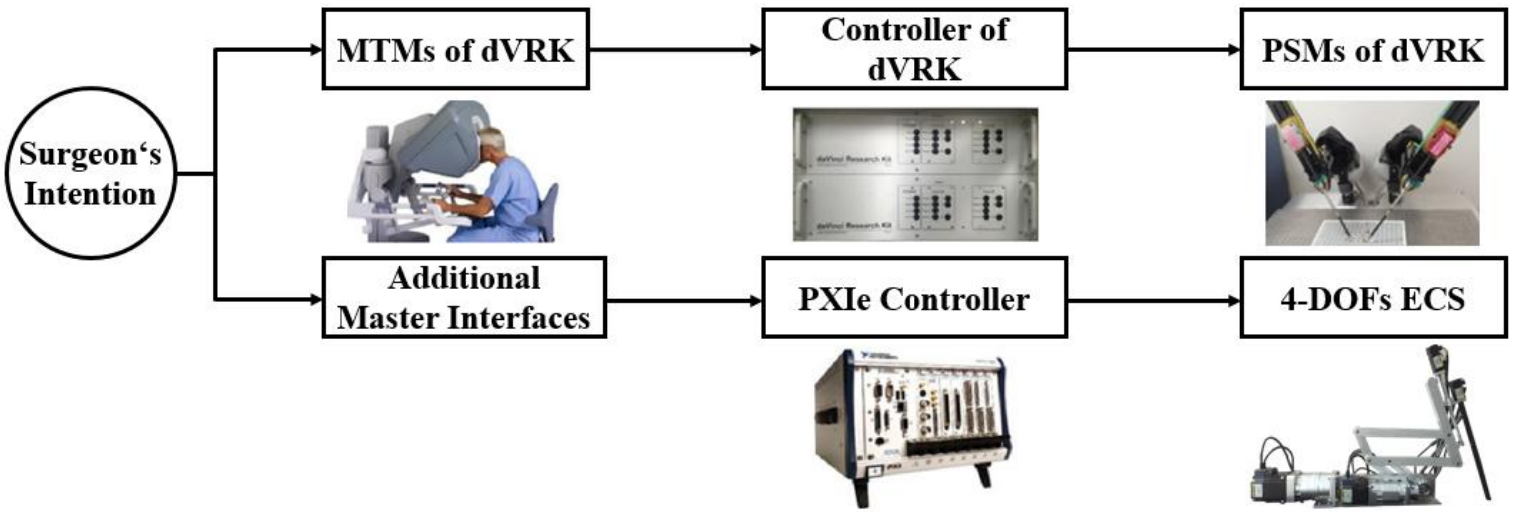

Fig. 2.14 Control flow of the proposed surgical robot system driven by the surgeon's intention. Software integration is based on the LabVIEW® software.

Simple 3D Endoscope

To provide 3D vision to the surgeon and thereby ensure safe robotic surgery, a simple 3D endoscope, which is not included in the dVRK system, was developed explicitly for the laparoscopic surgical robot system. This simple 3D endoscope consists of two CMOS camera modules with six built-in light-emitting diodes (LEDs) and is capable of generating images with a resolution of 640 × 480 pixels, aligned in parallel to procure 3D vision. However, because simply aligning the two image sensors physically does not eliminate distortion or misalignment between the two camera modules, the two acquired images undergo a stereo calibration process, in which the geometric relationship between the two image sensors is calibrated to place them on the same plane, and a stereo rectification process that places the two calibrated images on a common image plane. These processes provide precise 3D vision to the surgeon via the stereo viewer. More specifically, the stereo calibration process includes the homography-based and chessboard calibration methods. The former method produces multiple sets of extrinsic parameters and enables calculation of the image sensor's unique intrinsic and distortion parameters [67]. The latter method further improves the result by using chessboard [67]. Subsequently, stereo rectification is performed to horizontally align the two images and crop the effective image area, after which the reconstructed images are sent to the stereo viewer [68].

Through the above processes, the surgeon obtains 3D vision via the stereo viewer based on the calibrated and rectified images. In addition, the tip of the

developed endoscope is bent at an angle of 30 degrees to enable a wide vision range [69]. The outer case of the simple 3D endoscope is 10 mm in diameter and was manufactured based on rapid prototyping techniques (Form 1+, Formlabs, Somerville, MA, USA) with resolution to the nearest millimeter, as shown in Fig. 2.15.

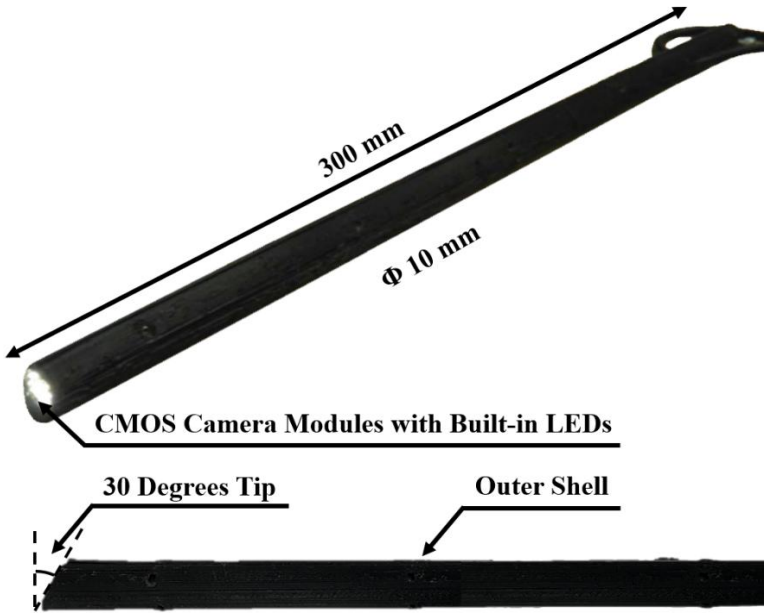

Fig. 2.15 Simple three-dimensional (3D) endoscope manufactured using 3D printing technique. Two complementary metal-oxide-semiconductor (CMOS) camera modules are used for reconstructing stereo view. 6 Built-in light-emitting diodes (LEDs) of each module is used as light source. The tip of the endoscope is developed to have 30 degrees to procure a wide range of view. The length and the diameter of the surgical instrument is designed as 300 mm and 10 mm, respectively.

Endoscope Control System

The 4-DOFs ECS with four controllable joints, *J1* to *J4*, controls the position of the simple 3D endoscope, as shown in Fig. 2.16. It uses four servo motors to provide the 4-DOFs, comprising rolling motion, pitching motion, yawing motion, and translational motion, to the ECS. Furthermore, a two-parallel link structure was adopted to control the position of the developed 3D endoscope with optimized fulcrum point motion, which is necessary for laparoscopic robotic surgery. Thus, the fulcrum point motion of the system is guaranteed by its hardware structure, not by a control algorithm. This means that it is able to provide a reliable and fixed fulcrum point motion, and therefore insure the patient safety.

As shown in the figure, the yawing motion of the 3D endoscope is provided by *J1* and the pitching motion by *J2* based on the bevel gear mechanism that transmits rotational motion at a 90 degree angle. The translational motion is generated by *J3*. More specifically, it is accomplished by male and female screw mechanism which converts the rotation motion to the translational motion. Actuation of the motor of *J3* rotates the male screw and consequently the female screw moves translationally along two parallel line guides placed on either sides of the male and female screw arrangement. The rolling motion is provided by *J4*, which connects the motor's shaft and the 3D endoscope via a customized coupler. Thus, the 4-DOFs ECS can perform the translational and fulcrum point motion during surgery by receiving the surgeon's control of the additional master interfaces.

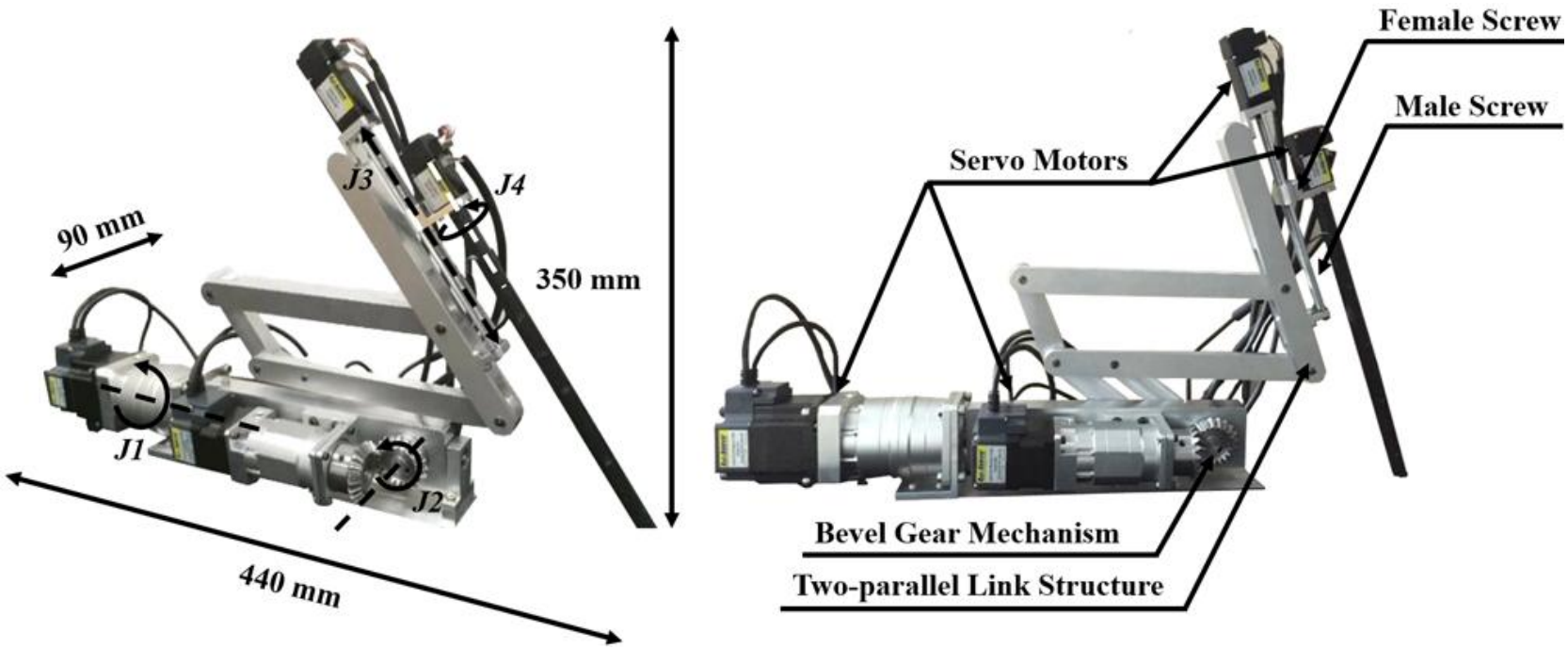

Fig. 2.16 4-DOFs endoscope control system (ECS). The fulcrum point motion is achieved by *J1* and *J2* with its two-parallel link structure. The translational motion and rolling motion are accomplished by *J3* and *J4*, respectively.

3. Results

3.1. Novel Master Interface with Application Systems

3.1.1. Novel Master Interface

Performance Test

The performance of the NMI was evaluated by intercepting the data it transferred using a specific LabVIEW® algorithm. The data transferred in both directions, along with the center push of the NMI were measured for 50 separate trials. No error occurred during these trials, indicating that the NMI can reflect the surgeon's decision with high precision.

Data Transfer Time

The data transfer time of the NMI was determined by physically connecting it to the universal serial bus port to enable it to send data via wired communication. Then, the NMI transferred data both to the wireless data

receiver and the universal serial bus port. The respective reception time for the data transferred through the two media types was each recorded using LabVIEW®. This experiment was repeated 10 times. The resulting data transfer time for both media types was found to be 132 ms on average with a standard deviation (SD) of 5 ms.

Power Consumption

Because the NMI is to be used during surgery, the amount of power it consumes has to be considered. As outlined above, the NMI utilizes a Li-MnO2 type Lithium button cell battery. To estimate the power consumption of the NMI, a LabVIEW® algorithm that continuously received data from the NMI and which recorded the time when the NMI stops the data transfer—inferring that the NMI was out of power—was developed. This experiment was executed 10 times. The results indicate that the power consumption of the NMI is 0.21 Wh (SD: 0.01 Wh). This means that the NMI can be operated for 185 min (SD: 9 min) without changing its power source. This is longer than the average time of several robotic surgeries [1, 4, 70, 71]. Moreover, because the button cell battery of the NMI can be easily replaced with a new one, for surgeries that extend beyond the time duration of the NMI, this would cause minimum inconvenience. Furthermore, the system would be safe even when the NMI has run out of battery since it would not send any data that can control the robotic assistant.

3.1.2. Robotic Assistant

Surgical Instrument

Gripping Force

A flexible piezoresistive sensor (Flexiforce, Tekscan Inc., South Boston, MA, USA), which is widely used in medical applications, was used to measure the gripping force of the proposed surgical instrument. The Flexiforce has been demonstrated to possess linearity [72]. Six precision weights (50, 100, 200, 500, 1000, and 2000 g) were used to calibrate the Flexiforce and transform the unit of the Flexiforce's output signal from voltage to Newton. These weights were measured using the Flexiforce in order 10 times based on LabVIEW®, and the output data were converted to force using the MATLAB linear regression method (MathWorks, Natick, MA, USA, using Seoul National University Academic License). Equation (3.1) shows the result of linear regression between the output voltage values and the force values:

$$F_{orce} = (1{,}592.70 \times V_{oltage} - 52.00) \times 9.81 \qquad (3.1)$$

To calibrate the measurement data and remove artifacts caused by the

environment, the initial 500 sets of data were collected and processed in each experiment. The measurement data for the gripping forces were recorded using a data acquisition board (USB-6212 DAQ, National Instruments, Austin, TX, USA). Following data acquisition, a Savitzky-Golay filter was applied to filter out sharp noise in the measured signal using MATLAB [73].

The gripping force was measured for every 0.05 revolution of the micromotor and the process repeated 10 times. Table 3.1 and Fig. 3.1 show the results of the relationship between gripping force of the surgical instrument and the revolution of the micromotor. The mean of all gripping forces' SD was computed as 0.51 N. The measurement data exhibited good linearity as the equation below:

$$GF_1 = c_1 R + i_1 \tag{3.2}$$

GF_1 (N) is the gripping force and R (rev) is the revolution of the micromotor. The coefficients: c_1 and i_1 of equation (3.2) were identified as 21.70 and 0.31, respectively. The coefficient of determination was calculated as 1.00. In this experiment, it was assumed that the physical properties of the Flexiforce and tissue are similar and thus the force applied on them would be also comparable.

Table 3.1 Repeated experimental results of gripping force measurements

Revolution of the micro motor (rev) \ Gripping Force (N)	Mean	Standard deviation
0	0	0
0.05	0.92	0.30
0.10	2.00	0.11
0.15	3.63	0.21
0.20	4.37	0.16
0.25	6.27	0.70
0.30	7.27	0.60
0.35	8.36	0.46
0.40	9.47	0.60
0.45	10.61	0.62
0.50	11.41	0.62
0.55	11.93	0.31
0.60	13.24	0.57
0.65	14.30	0.60
0.70	15.35	0.62
0.75	16.18	0.66
0.80	17.46	0.73
0.85	18.68	0.70

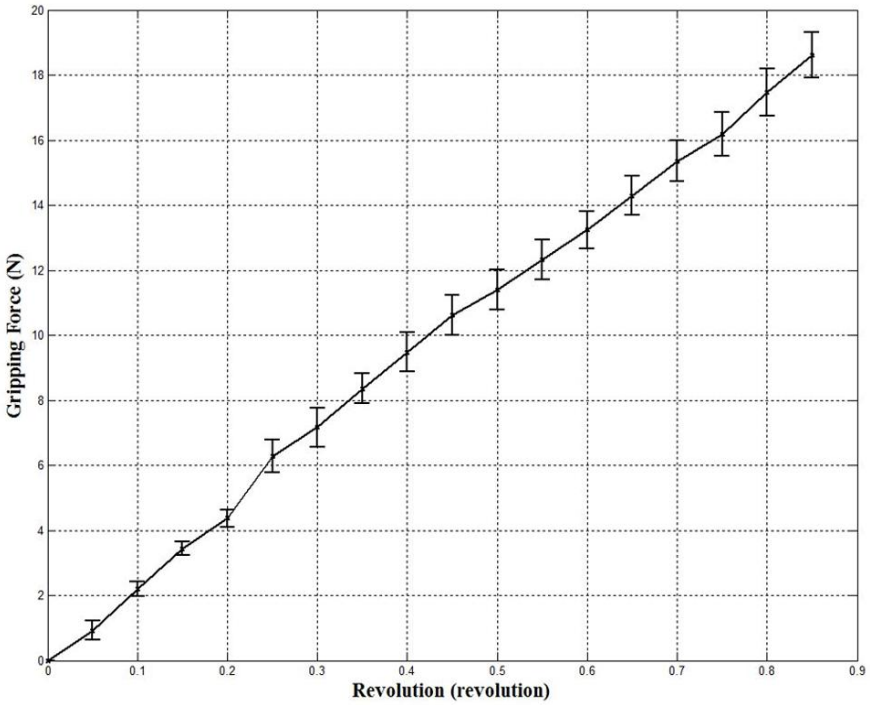

Fig. 3.1 Experimental results of gripping force compliant with position of the micro motor. The experiments repeated 10 times and the standard deviation is plotted as error bar. The interval of the position of the micro motor was 0.05 revs.

Reaction Time

The reaction time of the surgical instrument's gripping motion was estimated by performing a step function using its gripping force value. The performance result was then compared with the ideal step function after applying the Savitzky-Golay filter for the same reason as described above. For this experiment, a gripping force value of 4.37 N (SD: 0.16 N) was selected because performing the highest gripping force value for the purpose of the experiment is meaningless. The experiment was repeated 10 times with a 2 s time interval between every two gripping motions and the time duration of the gripping motion. For the experiment, a specific LabVIEW® algorithm was developed to ensure that the intervals between the gripping motions were precise. The results obtained show that the step function generated by the gripping motion and the ideal step function have close conformability. The calculated mean of the time delay was 0.4 s.

Durability Test

To test the durability of the surgical instrument, a LabVIEW® algorithm that continuously repeated the gripping motion was developed. The time intervals between every two gripping motions and the time duration of each gripping motion were set to 1 s. A gripping force of 4.37 N (SD: 0.16 N) was also selected in this experiment for the same reason as in the reaction time

experiment. The gripping motion was repeated 1000 times and the gripping force values during the repetitions recorded. The mean gripping force was found to be 4.23 N with SD of 0.13 N, which is within the SD of the initial gripping force value.

Workspace

The workspace of the proposed additional surgical robot arm system was calculated using the external robot arm's Denavit-Hartenberg parameter, inferred in previous research [2], and compared with the workspace required for cholecystectomy, as shown in Fig. 3.2. The calculated workspace was 8,397.4 cm^3, which exceeds the reference workspace [74], 549.5 cm^3.

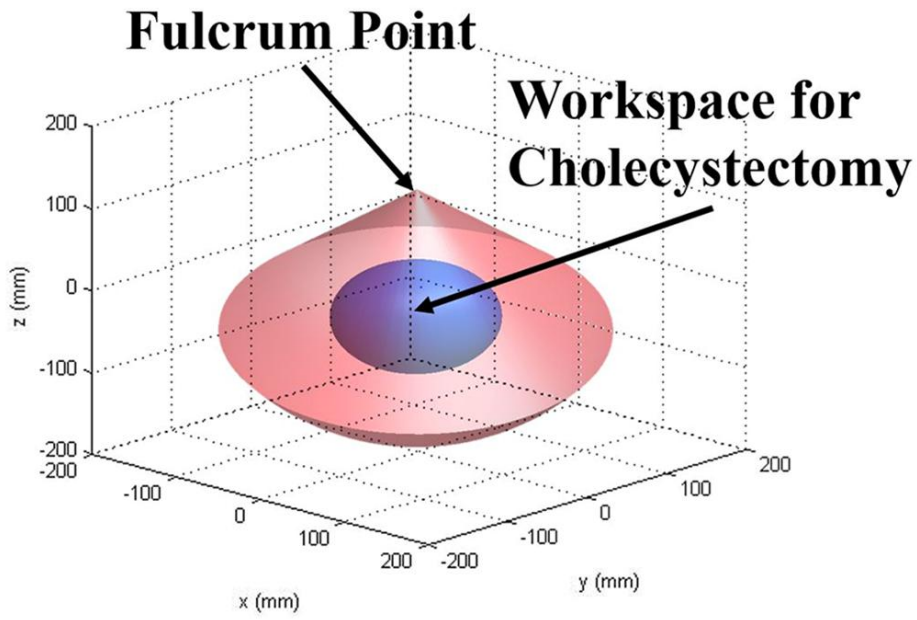

Fig. 3.2 Workspace of the proposed robotic assistant.

System Specification

Table 3.2 summarizes the proposed robotic assistant that consists of the additional master interfaces, external robot arm, and assistant surgical instrument.

Table 3.2 System specifications of the robotic assistant

Specification item	Unit	Joints	
Installing posture			Floor mounted
Construction			Vertical articulated type
Degrees of freedom			7
Drive method		J1 ~ J6	AC servomotor
		Gripper	Brushless DC motor
Arm length	mm		565 (external arm) + 300 (surgical instrument) = 865
Operation range	°	J1	±170
		J2	+135, -100
		J3	+166, -119
		J4	±190
		J5	±120
		J6	±360
Maximum speed	mm/s	J1 ~ J6	8,200
Position repeatability using additional master interface	mm	J1 ~ J6	±0.02
Gripper's gripping force	N		0 ~ 18.68
Gripper's reaction time	s		0.4
Entire system's workspace	cm^3		8,397.4
Motion scaling range	%		0 ~ 200
Gripper function			Gripping only
Sterilization			Not available

3.1.3. Novel Master Interface with Robotic Assistant

Simple Peg Task

To validate the peg transfer performance, fundamentals of laparoscopic surgery (FLS) peg transfer kit were used in the performance of a block transfer task which followed standard FLS curriculum except for the mid-air transfer since only one surgical instrument was used in this research. The system setup is shown in Fig. 3.3. For this experiment, three novice volunteers were recruited. They were asked to follow the process outlined below for the modified FLS block transfer task curriculum—already predefined in previous research for validation of surgical robot systems and measurement of the surgeon's technical skills and eye-hand coordination during surgery [2, 70, 74-76]. The process can be divided into the following two steps: (i) the volunteers were asked to transfer six objects from the left side of the board to the right side of the board and (ii) the time taken to transfer the six objects, between the volunteer picking up the first object and releasing the last object, was measured. The time limit was set to 300 s which was determined by FLS curriculum, the same as in other research [2, 70, 74-76]. The three volunteers executed three tasks each and the results show that the mean time of the peg

transfer task was 250 s with SD of 6 s, as summarized in Table 3.3. According to Table 3.3, all volunteers succeeded in the peg transfer task within the time limit, 300 s.

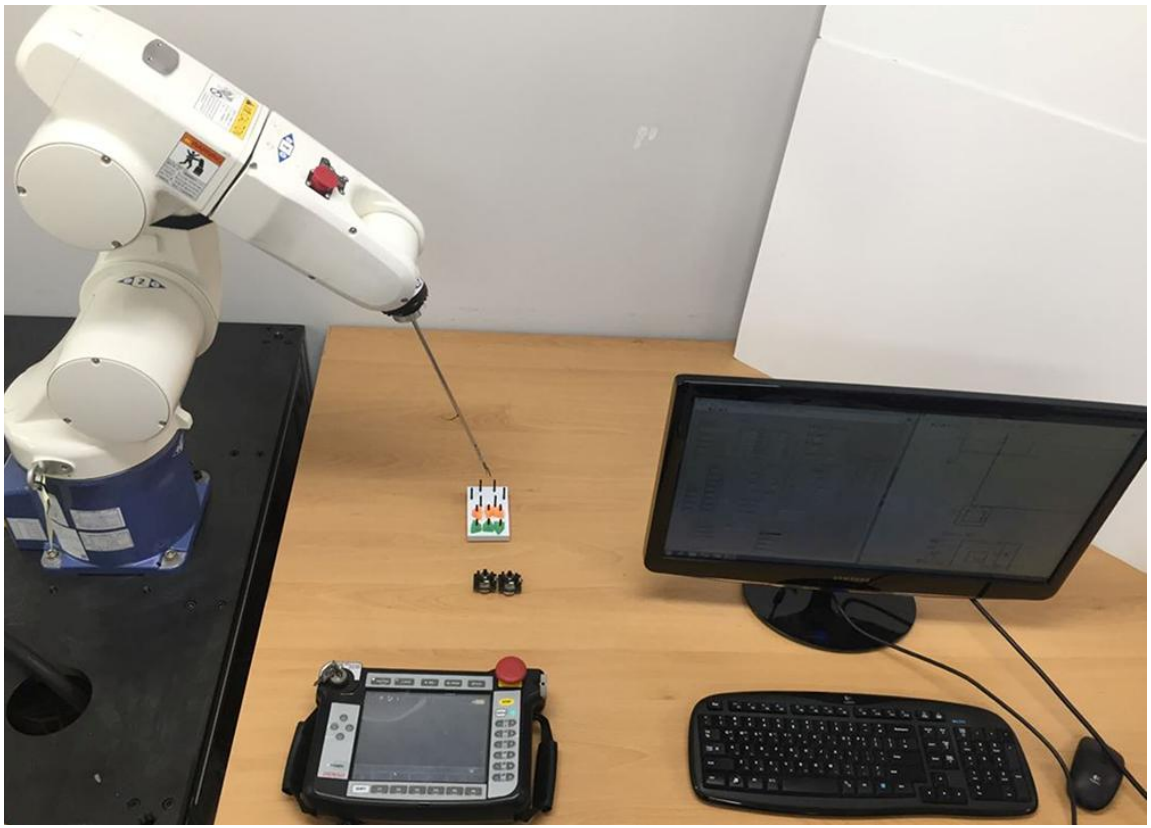

Fig. 3.3 System setup for the peg transfer task using fundamental of laparoscopic surgery (FLS).

Table 3.3 Execution time of block transfer task

Trial Number	Execution time (sec.)			
	Volunteer 1	Volunteer 2	Volunteer 3	Total Mean
1	242	268	260	257
2	231	261	253	248
3	226	264	246	245
Mean	233	264	253	250
SD	8	4	7	6

* Abbreviation: Standard Deviation (SD).

In vitro Test of Semi-automatic Resected Object Removal

To evaluate the performance of the robotic assistant as an assistant, which is the main purpose of this study, an *in vitro* test of semi-automatic resected object removal was performed. The setup for the test is depicted in Fig. 3.4. Three volunteers were recruited to perform the *in vitro* test. The process was as follows: (i) grasp and cut the rubber ring via the operation robot arm, (ii) then, grasp the cutted rubber ring using the robotic assistant in order to remove the resected object from inside the simulated peritoneum and (iii) once the surgical robot had grasped the object, the robotic assistant would switch to automatic mode to automatically take the object out of the simulated peritoneum. After the end of the surgical instrument was outside of the simulated peritoneum, it should put down the object and return to the operation area, and enable the volunteer to maneuver the robotic assistant.

To achieve the automatic mode described in the third step of the test, a built-in magnet was installed within the outer shell of the surgical instrument and located 6 cm away from the tool tip of the surgical instrument, as shown in Fig. 3.4-(b), and a magnetic sensor (WSH138-XPAN2, Winson, Taiwan) that could linearly transform the detected magnetic force into voltage value was attached to the simulated trocar, as shown in Fig. 3.4-(c).

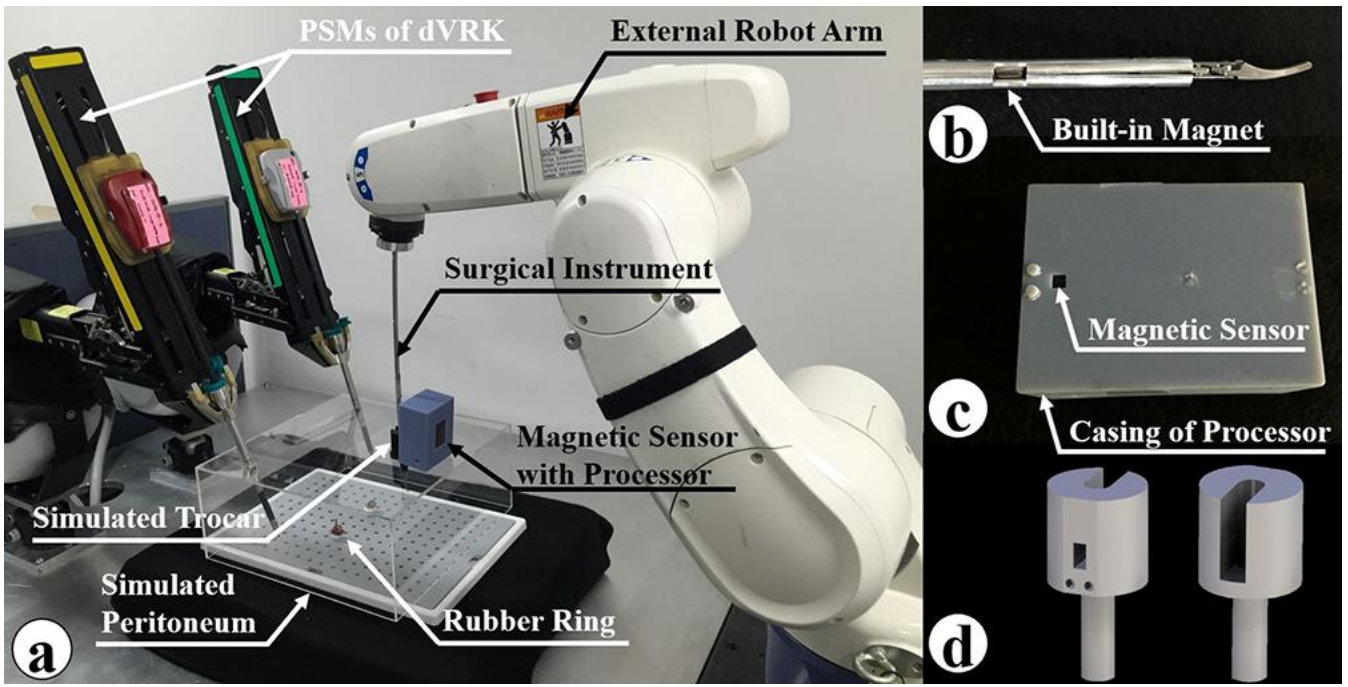

Fig. 3.4 Setup for the *in vitro* test of semi-automatic resected object removal. (a) Overall system setup. (b) Built-in magnet of the surgical instrument to generate magnetic field. (c) Magnetic sensor with its controller board within the special housing. (d) Developed simulated trocar used in the *in vitro* test.

An Arduino-based microcontroller board (ATmega328, Atmel, San Jose, CA, USA) was used to receive the voltage data transformed by the magnetic sensor, and a special housing was manufactured to attach the microcontroller board to the simulated trocar, as shown in Fig. 3.4-(c). The simulated trocar was developed to install the magnetic sensor and enable the surgical instrument to get rid of the resected object, as shown in Fig. 3.4-(d). To convert the data from voltage to distance, the voltage value was measured using the magnetic sensor for every 0.2 cm of the distance between the magnet and the magnetic sensor and the process repeated 10 times. As a result, the measurement data showed good linearity as the equation below:

$$D = c_2 \times V + i_2 \tag{3.3}$$

D (cm) is the distance between the magnet and the magnetic sensor and V (mV) is the voltage value measured by the magnetic sensor. The coefficients: c_2 and i_2 of equation (3.3) were identified as −0.10 and 70.10, respectively. The coefficient of the determination was calculated as 1.00. The maximum distance that can be sensed by the magnetic sensor is 2 cm.

Thus, by sensing the magnetic field generated by the surgical instrument's built-in magnet based on the microcontroller board and the magnetic sensor, it was able to notify the system of the distance between the end of the end-

effector and the simulated trocar. Then, the robotic assistant was commanded to translationally move 6 cm from the moment that the detected distance equal to zero which would result in the end of the end-effector is on the simulated trocar. In such a case, the surgical instrument would abandon the resected object and return to the operation area. Consequently, the third step of the *in vitro* test could be operated automatically. The control flow of the automatic mode is outlined in Fig. 3.5.

Each volunteer repeated the *in vitro* test three times. All the volunteers were able to successfully remove the resected object using the robotic assistant. Further, no collision occurred between the operation arm and the robotic assistant during any of the tests.

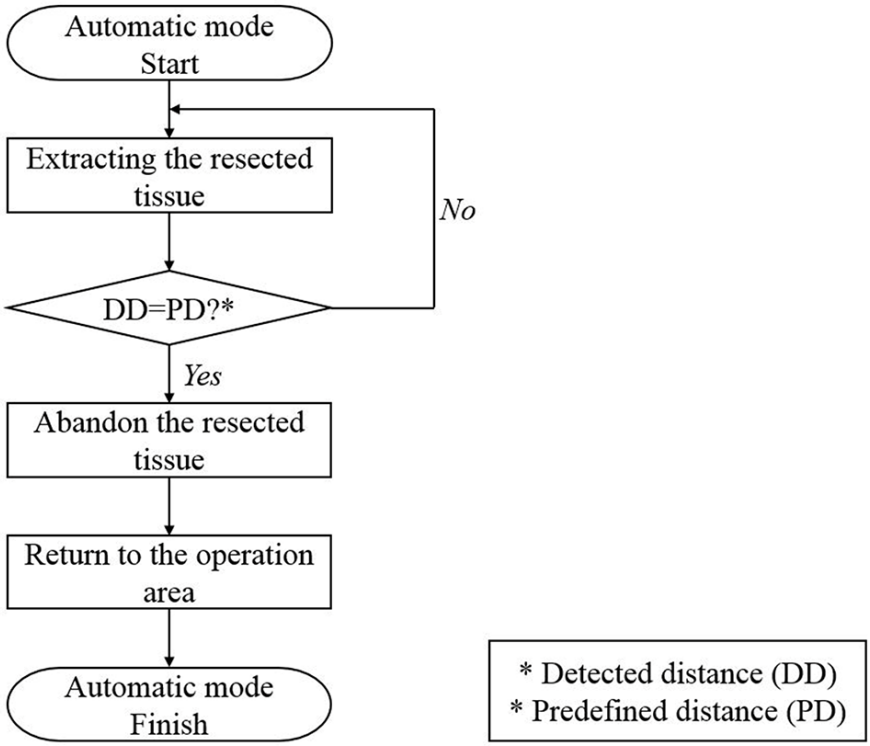

Fig. 3.5 Control flow of the automatic mode needed in the *in vitro* test

3.1.4. Stereo Endoscope System

Simple 3D Endoscope

Fig. 3.6 shows the results of the stereo calibration and rectification process using the chessboard. As shown in Fig. 3.6-(a), the original images obtained by the two image sensors are distorted and misaligned, which means that the surgeon would not be able to comprehend them if they were simply projected onto the stereo viewer. Therefore, the stereo calibration process calculates intrinsic parameters such as distortion coefficients and then the two images are calibrated, as shown in Fig. 3.6-(b).

The stereo rectification results can be seen in Fig. 3.6-(c). The green lines in the figure are horizontal lines in the images for aligning the two images to the same height. The pink boxes represent the effective image area for stereo view. The effective image area of the obtained images are cropped and reconstructed for providing a clean stereo view to the surgeon.

Fig. 3.7 shows the original images and the final images provided to the surgeon after above processes.

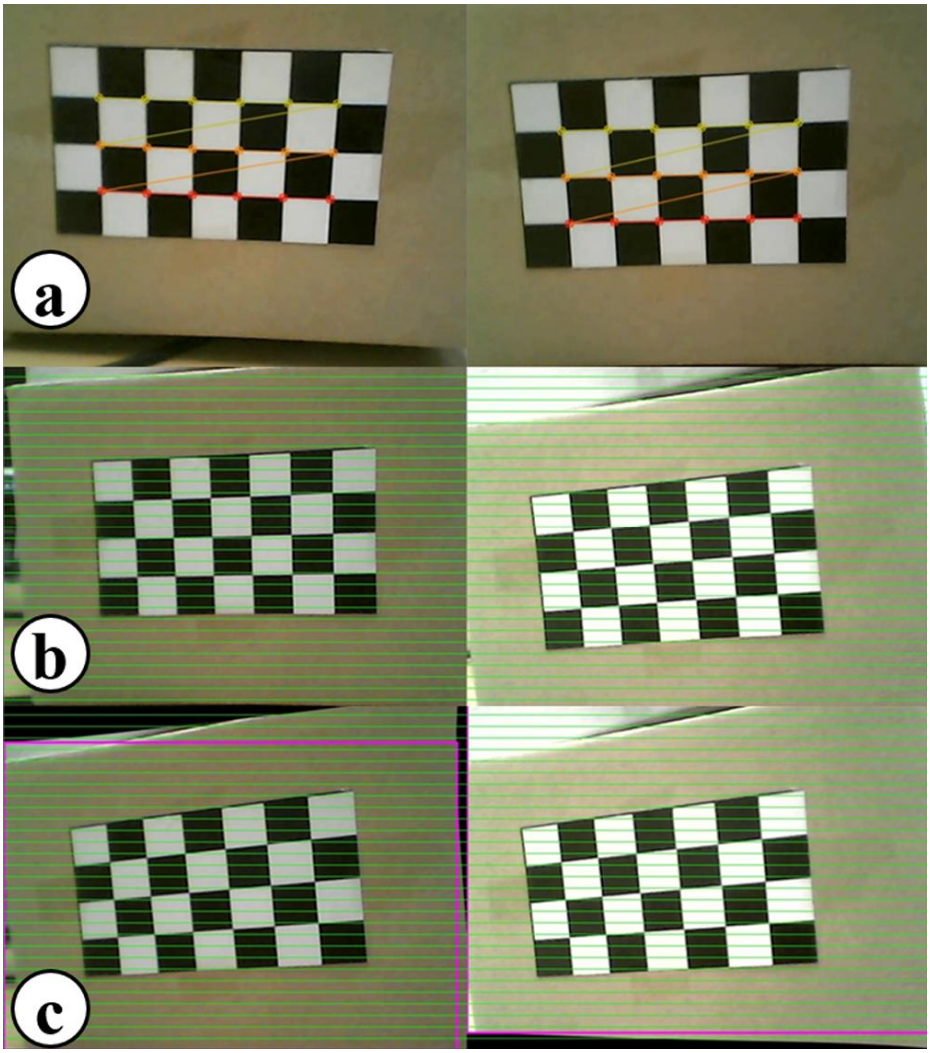

Fig. 3.6 Stereo calibration and rectification processes. (a) Stereo calibration process. (b) Stereo rectification process. (c) Calibrated and rectified images with effective area enclosed in a pink box.

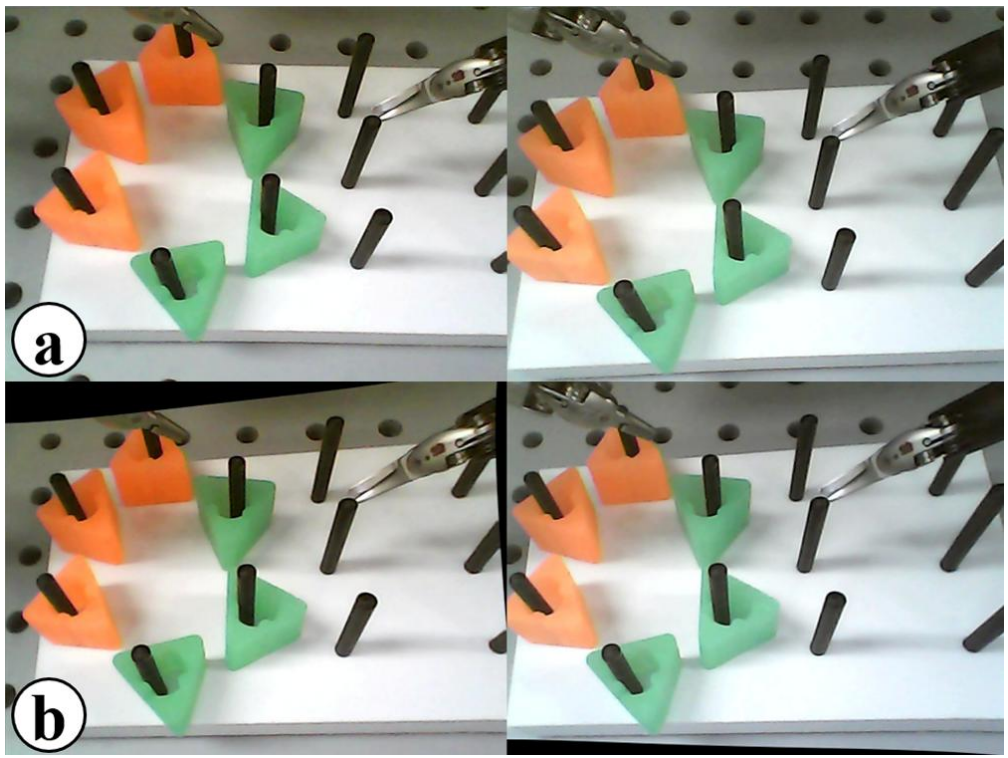

Fig. 3.7 Comparison between original images and final images. (a) Original images obtained. (b) Final images after stereo calibration, rectification, and reconstruction.

Workspace

The workspace of the proposed 4-DOFs ECS was calculated based on the hardware design of the system, and compared with the workspace required for cholecystectomy, as shown in Fig. 3.8. The calculated workspace is 20,378.3 cm^3, which exceeds the reference workspace [74] of 549.5 cm^3.

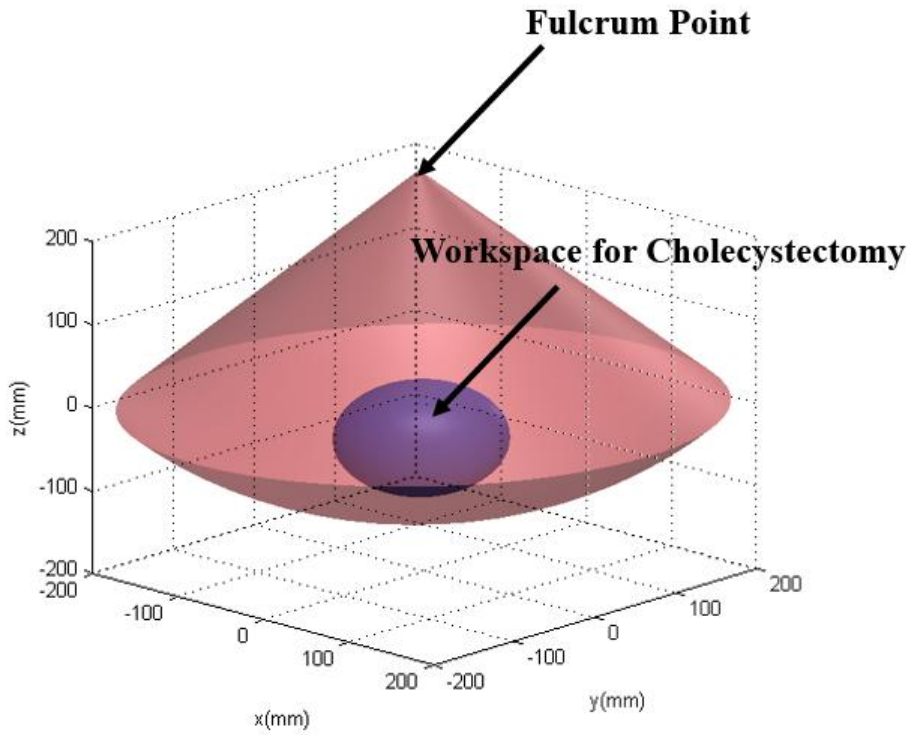

Fig. 3.8 Workspace of the proposed 4-DOFs ECS.

System Specification

Table 3.4 summarizes the system specifications for the developed 4-DOFs ECS.

Table 3.4 System specifications of the 4-DOFs ECS

Specification item	Unit	Joints	
Installing posture			Floor mounted
Construction			Two-parallel link structure
Degrees of freedom			4
Drive method		J1 ~ J4	Closed loop stepping system
Operation range	°	J1	±45
		J2	±60
		J4	±360
	mm	J3	160
Maximum speed	rpm	J1, J2, J4	3,000
	mm/s	J3	50
Position repeatability using additional master interface	mm	J1 ~ J4	±0.1
Entire system's workspace	cm^3		20,378.3
Sterilization			Not available

3.1.5. Novel Master Interface with Stereo Endoscope System

Modified Peg Transfer Task

To validate the overall performance of the proposed laparoscopic surgical robot system, a peg transfer task was designed and performed using a newly developed peg transfer board redesigned based on the FLS peg transfer kit, as shown in Fig. 3.9. The peg transfer board was modified because the standard FLS peg transfer board does not require the endoscope system to be manipulated owing to its relatively small size, and therefore it is not able to evaluate the proposed surgical robot system consisting of the additional master interfaces, simple 3D endoscope, and 4-DOFs ECS, which requires manipulation of the endoscope system. Then, the FLS peg transfer task curriculum, which has already been defined in previous research for validation of surgical robot systems and measurement of the surgeon's technical skills and eye-hand coordination during surgery [2, 70, 74-76], was performed using the new peg transfer board. Three novice volunteers were recruited for the tasks and followed next steps: i) the volunteers were asked to transfer six objects from the left side of the board to the right side of the board and ii) the time taken to transfer the six objects, between the volunteer picking up the first object and releasing the last object, was measured. In addition,

during the task, the volunteers were requested to always ensure that all surgical instruments were in view to mimic an actual surgical environment where safety has to be ensured. Furthermore, this is also one of the standards to evaluate the robotic surgical skills of the surgeon. The number of surgical instruments obscured from view was also counted during the experiments. The system setup is shown in Fig. 3.9. The stereo viewer was used for the task and the obtained calibrated and rectified images projected onto the stereo viewer to provide 3D vision to the users. Same with other studies, the time limit of the experiment was also set to 300 s in spite of the relatively long peg transfer board and use of the stereo viewer [2, 70, 74-76]. This time limit was also provided by FLS curriculum.

Each of the recruited three volunteers performed three tasks. As a result, the mean time of the peg transfer task was 267 s with SD of 6 s and the surgical instruments were always in view during the task, as summarized in Table 3.5. According to Table 3.5, one volunteer failed to perform the modified peg transfer task within the 300 s, which is the time limit. To evaluate the effectiveness of the NMI in more detail, a similar peg transfer task was performed by the three volunteers but they were not allowed to manipulate the NMI and the MTM simultaneously—in order to mimic the swapping of control of the current surgical robot system. The results of the task are summarized in Table 3.5. As can be seen in Table 3.5, execution times of the tasks were evidently increased and all volunteers failed to finish the task within the time limit of 300 s. Furthermore, in this case, the surgical

instruments were at times out of sight.

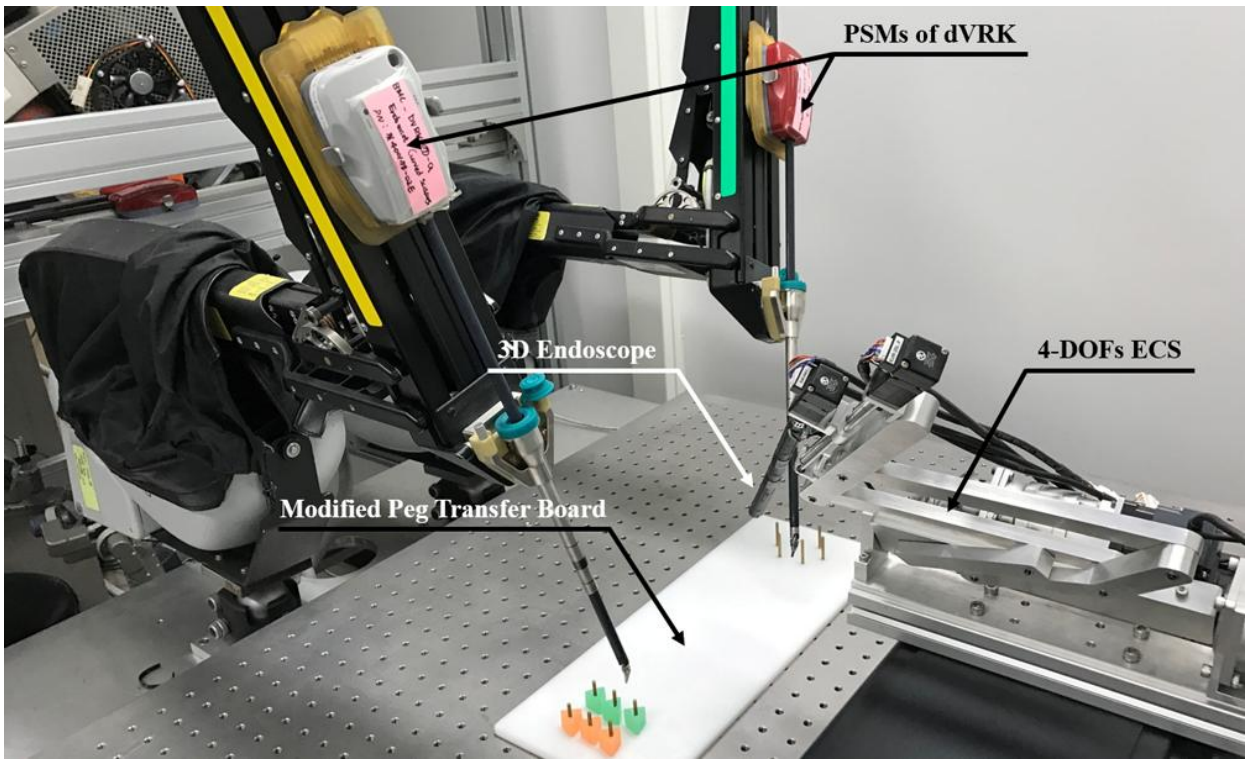

Fig. 3.9 System setup for the modified peg transfer task. Modified peg transfer board was developed and used for the task to evaluate the overall performance of the proposed system.

Table 3.5 Execution time of modified peg transfer task using the NMI

	Trial Number	Execution time (sec.)			
		Volunteer 1	Volunteer 2	Volunteer 3	Total Mean
Allow Simultaneous Operation	1	308	255	245	269
	2	327	253	237	272
	3	300	248	234	261
	Mean	312	252	239	267
	SD	14	4	6	6
Forbid Simultaneous Operation	1	387	363	346	365
	2	353	336	314	334
	3	331	318	306	318
	Mean	357	339	322	339
	SD	28	23	21	24

3.2. improved Novel Master Interface with Application System

3.2.1. improved Novel Master Interface

Performance Test

A specific LabVIEW® algorithm, which is able to receive coordinate information of touched touch sensor and generated gesture information, was developed to estimate the precision of the iNMI. This was then achieved by receiving the data generated by the iNMI includes touch status of total 25 touch sensors and generated gesture motion for controlling the endoscope system, such as upward swipe, downward swipe, forward swipe, and backward swipe. The coordinate of touched sensor and gesture information were separately tested and repeated 50 times. Then, every signal was checked to verify the iNMI is able to correctly reflect user's intent. No error detected during the repeated tests, which indicates that the iNMI is able to receive the surgeon's decision with high correctness.

Data Transfer Time

To evaluate the latency of the iNMI, the data generated by the iNMI were transferred by both wired communication and wireless communication. Wire communication was used as reference data transfer time and performed by physically connecting the iNMI using the universal serial bus port, more specifically, the universal serial bus port 2.0 type A. Therefore, the data transfer times of both types of communication were recorded using a specific LabVIEW® algorithm. Then, the difference of received time of two data transfer times, which can be regarded as latency due to the iNMI's wireless communication, was calculated. During the test, gesture motion was generated and transferred by the iNMI. Furthermore, the gesture information has been encoded into 1 byte number for minimizing the data transfer time. The latencies were measured for 50 times and the results shown that the latency of the iNMI was 5 ms on average, with a SD of 1 ms.

Power Consumption

The power consumption of the iNMI is highly significant since it is to be used during surgery. To evaluate the power consumption, a LabVIEW® algorithm was developed to continuously intercept the data produced by the iNMI and record the time when there is no any data received, which indicates the iNMI was out of power. The tests were performed for 10 times. The results indicate

that the power consumption of the iNMI is 0.12 Wh (SD: 0.01 Wh) and it is able to operate for 317 min (SD: 12 min), which is much longer than the average time for several types of robotic surgeries [1, 4, 70, 71]. However, the iNMI can also be used for surgeries which exceed its time duration since the battery can be simply changed to a new one which would cause minimum inconvenience. The iNMI is safe even when the iNMI battery has no power because it would not send any data that can control the ECS.

3.2.2. improved Novel Master Interface with Stereo Endoscope System

Modified Peg Transfer Task

To evaluate the overall performance of the proposed stereo endoscope system with the iNMI. Modified peg transfer task was performed under a perfectly same condition. The results of the task are summarized in Table 3.6. As can be seen in Table 3.6, execution times of the tasks were clearly reduced when it compare with the result with the NMI.

Table 3.6 Execution time of modified peg transfer task using the iNMI

	Trial Number	Execution time (sec.)			
		Volunteer 1	Volunteer 2	Volunteer 3	Total Mean
Allow Simultaneous Operation	1	285	223	204	237
	2	263	187	197	216
	3	198	185	191	191
	Mean	249	198	197	215
	SD	37	17	5	19
Forbid Simultaneous Operation	1	330	287	295	304
	2	308	289	271	289
	3	286	254	289	276
	Mean	308	277	285	290
	SD	18	16	10	11

4. Discussion

Robotic surgery, an attractive alternative to conventional open and laparoscopic surgery, has been in clinical practice for many years. However, current operation room for robotic surgery is too messy and therefore still needs improvement. To resolve this issue, compact type HOTAS controllers were developed and adopted to current master interface of laparoscopic surgical robot system. The purpose was to help surgeons perform additional surgical operations and thereby overcome current situation of operation room, just as the number of pilots inside the cockpit was reduced from two to one with the advent of HOTAS controller. With this purpose, the NMI was developed to be installed to each of the MTMs of the dVRK system. The performance of the NMIs was evaluated via an experiment that was repeated 50 times with no error occurring. The results of the latency and power consumption experiments showed that the motions of the proposed application systems are able to act on the decision of the surgeon in 132 ms via the NMI, which can be regarded as a real-time system [77], and the power capacity can cover several types of surgeries. Further, even if the power source might not be durable for the whole time of long surgeries, the NMI is still effective because its power source can be easily replaced. These experimental results demonstrate that the NMI can be used to reflect the surgeon's decision wirelessly and to manipulate the application systems

without errors.

After this, to resolve existing issues and provide more intuitive control, the iNMI was then developed. To estimate the performance of the iNMIs, the performance test was designed and repeated 50 times where no error was detected. The results of the data transfer time and power consumption experiments indicate that the motions of the proposed application systems are in accordance to the surgeon's intent in 4 ms via the iNMIs. This can be considered as real time [77], and the power capacity is sufficient for various kinds of surgeries. Moreover, since the power source of the iNMI can be simply replaced, the iNMI is still effective for those surgeries which exceed power volume of the iNMI. These experimental results indicate that the iNMI is able to precisely reflect the intent of surgeon and manipulate the application systems without errors.

Furthermore, two application systems that can be controlled using the additional master interfaces were proposed.

Firstly, the robotic assistant was proposed. The additional master interfaces were respectively attached to each of the MTMs of the dVRK system to enable simultaneous manipulation of the robotic assistant. The robotic assistant was developed by integrating the 6-DOFs external robot arm and the surgical instrument. The results of repeated gripping force of the surgical instrument indicate that the gripping force is comparable to that of conventional systems [2, 78, 79]. In addition, because the relationship

between the micromotor's revolution and the generated gripping force show good linearity with 1.00 of the coefficient of determination, the gripping force of the surgical instrument could be sensitively controlled by adjusting the micromotor's position. The reaction time of the surgical instrument's gripping motion was determined to be 400 ms. Thus, the total time delay from the surgeon giving the command to the surgical instrument actually gripping the object is 532 ms, which cannot be considered as a perfect real-time control due to its relatively long time delay. However, the gripping motion is still effective since the time delay around 500 ms is acceptable for surgical performance and can be adapted by human [80-83]. Furthermore, since the main cause of the time delay of the surgical instrument is the micromotor's speed, which was set to 75 % of the maximum speed during the experiment, the time delay would be shorter if the speed of the micromotor was increased. The results of 1000 on and off motions to check the durability of the surgical instrument show that the effect on the surgical instrument's force value was negligible. This experiment was adopted from previous research [2] because the durability of the surgical instrument developed cannot be tested based on the number of surgeries, as done in the case of the EndoWrist. For the final important step in the evaluation of the surgical instrument, the sterility issue has to be considered. Thus, sealing of the surgical instrument developed is planned for future work. As illustrated in Fig. 3.8, the workspace of the robotic assistant was calculated using the joint information of the 6-DOFs external robot arm [2]. The cone-like shape of the calculated workspace is a

result of the fulcrum point motion of the surgical robot system. Because the workspace is much larger than the cholecystectomy workspace, the robotic assistant is expected to be able to perform many types of surgeries whose workspaces can be covered by the cholecystectomy. Furthermore, the size of the calculated workspace can be increased by adjusting the limits of the range of movement of the 6-DOFs external robot's arm joints.

The resulting mean time and SD of the simple peg tasks were shorter than those of other similar systems using the same FLS kit and following the same FLS peg transfer task curriculum to validate their systems, where the execution times were even longer than 400 s. This demonstrated that a good performance and effectiveness can be provided by the proposed robotic assistant [2, 70, 74-76]. Furthermore, as shown in Table 3.3, the mean of each peg task's execution time was gradually decreased. This can be interpreted that the volunteers quickly adapted to the system and therefore showed a better result trial by trial. However, the mean and SD of each peg task's execution time were slightly longer when compared with the results using dVRK [2], which used only one MTM with one PSM and followed the same FLS peg transfer task curriculum using the same FLS peg transfer kit. The major cause of this result is the relatively slow speed of the external robot arm. Therefore, the results can be improved by developing a more stable control algorithm for the proposed system to enable higher speed.

The *in vitro* test of semi-automatic resected object removal indicated that the recruited volunteers were able to manipulate both of operation robot arms and robotic assistant. Moreover, no collisions occurred during the tests. This means that using the proposed robotic assistant, the surgeon can simultaneously perform the role of assistant to prevent collision between the operation robot arm and the assistant instrument.

However, due to the involvement of the external robot arm, there is possibility for the collisions between PSMs and the external robot arm. Thus, there is need to calculate the external robot arm's workspace with respect to two PSMs. For a more accurate calculation, trocar positions for robot-assisted laparoscopic bariatric surgery, which are also used for gastroesophageal reflux procedure, were used [84]. This is because the surgery also requires for a trocar used by the assistant. Furthermore, the postures of the two PSMs were set to be closest to the external robot arm for creating an extreme condition to the external robot arm's workspace, as shown in Fig. 4.1-(a). The endoscope has been excluded from consideration since the trocar position of the endoscope is even behind those of the PSMs [84] and its posture would not be toward the PSMs considering the operation area. The workspace has been calculated based on the measurement data of the PSMs and the external robot arm, such as actual dimension and maximum angle of motion. Under the assumption that the postures of the PSMs closest to the external robot arm using the maximum angle of motion data, the external robot arm performed

virtual remote center of motion while detecting the interference between the external robot arm and the PSMs. The workspace was then obtained by calculating the area without any interference which infers a collision-free area. As a result, the workspace for this condition was calculated to be 386.4 cm^3, which could cover 70 % of the workspace for cholecystectomy, as shown in Fig. 4.1-(b). Therefore, the external robot arm's workspace with regard to two PSMs can be also deemed to be sufficient considering the condition for above workspace was set to be extreme and it does not require for an entire workspace for cholecystectomy to remove a resected object. This also implies less possibility for collision since no complex control would be commanded to a robotic assistant. However, an auto collision avoidance system based on optical tracking system and motion planning algorithm is currently planning to be conducted for completely resolving above issue.

Using the proposed surgical robot system, with its SOBW-type surgical instrument, NMI based on HOTAS, and the dVRK system, surgeons will be able to execute the functions of an assistant and thereby avoid collisions without having to stop surgical operations.

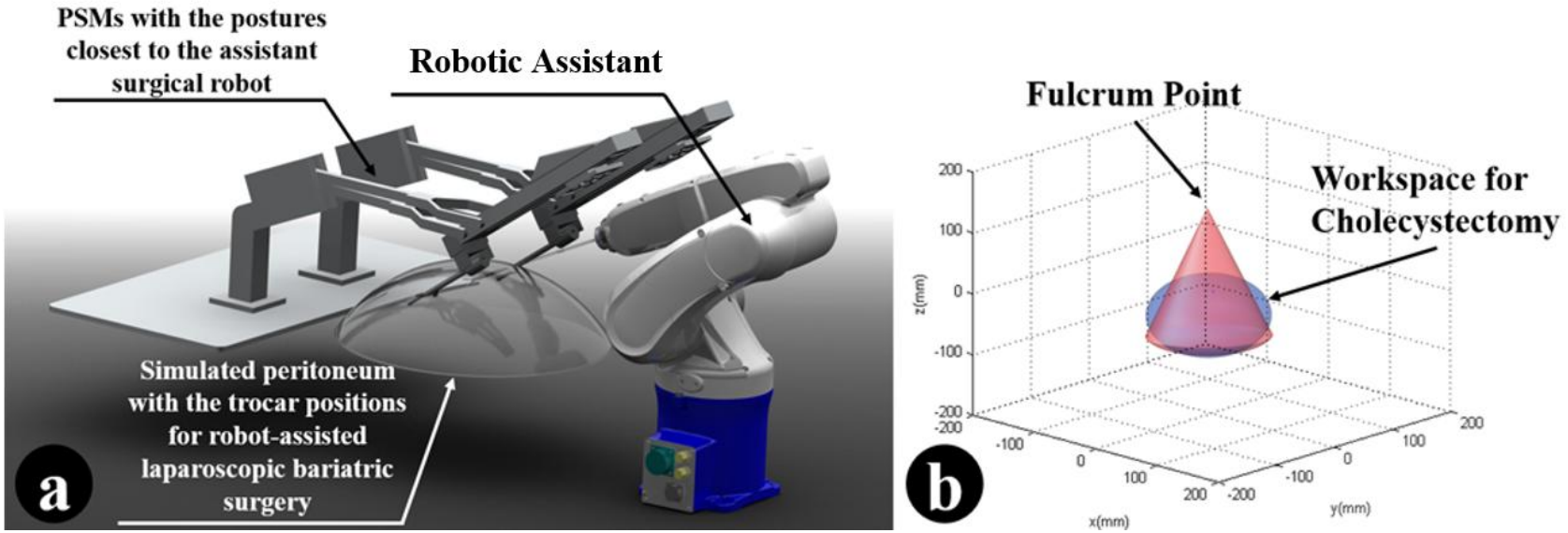

Fig. 4.1 Workspace analysis of the proposed robotic assistant with regard to PSMs. (a) An extreme condition to the robotic assistant's workspace. (b) Calculated workspace in the extreme condition

Secondly, the stereo endoscope system was proposed for providing continuous surgical flow and therefore decrease operation time and surgeon fatigue. Moreover, this would also result in collision between surgical instruments, injury to patient (from surgical instrument being out of sight), and having to endure an unsatisfactory view to avoid swapping control.

To enable continuous surgical operation by enabling simultaneous manipulation of the 4-DOFs ECS and PSMs, two additional master interfaces were installed to two MTMs of the dVRK system.

The developed simple 3D endoscope provides 3D vision by processing the acquired images using a stereo calibration and rectification algorithms. The volunteers recruited for the experiments used the stereo viewer, which displays two stereo images each on its left and right monitors, to obtain 3D vision during the task. All volunteers were able to determine distances and depths of objects on the provided view and execute the experiments.

As illustrated in Fig. 3.8, the workspace of the 4-DOFs ECS was calculated using its joint information. The shape of the estimated workspace, which is a cone-like shape, indicates the fulcrum point motion of the system. This was stably accomplished by its hardware structure rather than a software algorithm. Therefore, the proposed system provides a reliable and steady fulcrum point motion during robotic surgeries. The 4-DOFs ECS can be used for various kinds of surgeries which have smaller workspaces than that of the cholecystectomy since the system's workspace is much larger than the

cholecystectomy workspace. In addition, the calculated workspace can be further increased by adjusting the scale of the 4-DOFs ECS because it is manufactured with a relatively small size compared with the PSM. The resulting mean times of the modified peg transfer tasks with the iNMI were within the time limit of the FLS peg transfer task, even when the longer peg transfer board was used for the experiments in order to involve endoscope movements. This demonstrates that good performance is provided by the proposed surgical robot system using the iNMI, 4-DOFs ECS, and simple 3D endoscope. The comparison between the results with the NMI and iNMI can be shown in the Fig. 4.2. The gradually decreased execution time of each modified peg transfer task, as shown in Tables 3.5 and 3.6, can be inferred as the volunteers were able to rapidly adapt to the system. In addition, the execution time of the peg transfer task and the number of surgical instruments obscured from view demonstrably increased when simultaneous operation of the MTM and the iNMIs was not possible. This indicates that the discontinuous surgical flow would indeed result in longer surgical operation time and collisions between instruments or injury to patients caused by the surgical instruments being obscured from view.

Using the proposed system, consisting of the iNMI based on HOTAS concept, simple 3D endoscope, 4-DOFs ECS, and dVRK system, surgeons will be able to simultaneously operate the PSM with the 4-DOFs ECS, and thereby ensure continuous surgical flow, which will result in safer robotic surgery environments and decreased operation time. The current 4-DOFs ECS can be

only used as research purpose because of its relatively small size compared with actual endoscope system. However, the size of the system can be simply scaled-up to be used for real surgery. The sealing of 4-DOFs ECS is planned to be performed in the future for solving sterility issue [85].

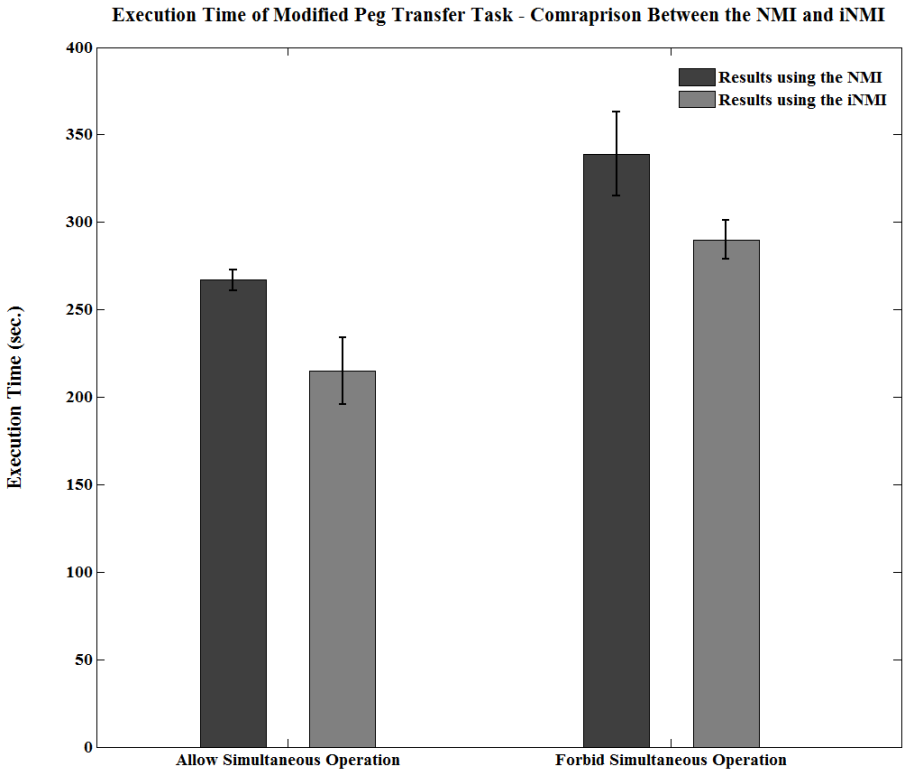

Fig. 4.2 Comparison between peg transfer task results using the NMI and iNMI (Error bar stands for standard deviation).

5. Conclusion

Robot-assisted laparoscopic surgery is a very desirable surgical operation because it provides several benefits compared with open surgery and conventional MIS. However, a major issue with robotic surgery has been the increased complexity of operation room which should be improved.

In this research, consequently, additional master interfaces that can be attached to the master interface of current da Vinci surgical robot system were proposed based on HOTAS controller which is used for flight control in the aerospace field and can control hundreds of functions and provide feedback to the pilot about flight conditions. Just like the arrival of HOTAS enabled less complex cockpit environment, it can be used to help surgeons perform additional surgical operations and thereby overcome current situation of operation room.

For this purpose, a wireless communication interface designed based on the HOTAS concept, called NMI, facilitates simultaneous manipulation of the operation robot arm and application systems. In this study, a tiny piece of hardware was developed to be attached to the MTM of the dVRK system, which was used as the operation robot. The results of performance tests, data transfer time experiments, and a power consumption test have confirmed that the proposed NMI is feasible & effective. In addition, the iNMI was consequently developed also based on HOTAS concept in order to enables

simultaneous and more intuitive manipulation of the application systems. The results of power consumption tests, latency experiments, and performance tests demonstrate that the proposed iNMI is practicable and effective.

Using the additional master interfaces, two application systems were also proposed.

Firstly, a robotic assistant that can be simultaneously manipulated by the surgeon via a wireless controller has been proposed. The robotic assistant comprises a surgical instrument with a diameter of 6 mm and 6-DOFs external robot arm. The surgical instrument uses a micromotor to generate gripping motion and the external robot arm can perform translational, fulcrum point, and rolling motions with the surgical instrument. The surgical instrument, which is based on SOBW, was validated via a gripping force experiment, a reaction time test, and a durability test. The workspace of the robotic assistant has clinical applicability. The results of a simple peg task and an *in vitro* test using the dVRK system have also indicated that the proposed system can be utilized in various types of laparoscopic robotic surgeries. However, the sterility issue needs to be resolved for the clinical application and this issue will be handled as future work.

This research also presented a stereo endoscope system consists of a 4-DOFs ECS and a simple 3D endoscope that can be controlled with proposed additional master interfaces. The 4-DOFs ECS uses four servo motors to generate pitching, yawing, rolling, and translational motion based on SOBW

concept. The fulcrum point motion, which is necessary for the laparoscopic surgical robot system, is achieved by adopting a two-parallel link structure. The workspace of the 4-DOFs ECS is shown to have clinical applicability. The simple 3D endoscope, which has a diameter of 10 mm, was developed using two CMOS camera modules with six built-in LEDs. The two images acquired by the image sensors undergo stereo calibration and rectification to provide a clear stereo vision, and reconstructed stereo images are provided to the user via the stereo viewer of the dVRK system to enable 3D vision during surgery. Further, the results of a modified peg transfer task indicate that the proposed system is able to provide continuous surgical operation and therefore remove the issues affecting surgical robot systems. The size of the 4-DOFs ECS can be simply scaled-up for being used in clinics and the sealing issue will have to be resolved in order to overcome sterility issue.

References

[1] Pahwa M, Pahwa AR, Girotra M, Abrahm RR, Kathuria S, Sharma A. Defining the pros and cons of open, conventional laparoscopy, and robot-assisted pyeloplasty in a developing nation. Adv Urol. 2014;2014:850156.

[2] Lee C, Park WJ, Kim M, Noh S, Yoon C, Lee C, et al. Pneumatic-type surgical robot end-effector for laparoscopic surgical-operation-by-wire. Biomed Eng Online. 2014;13:130.

[3] Kang BH, Xuan Y, Hur H, Ahn CW, Cho YK, Han S-U. Comparison of surgical outcomes between robotic and laparoscopic gastrectomy for gastric cancer: The learning curve of robotic surgery. J Gastric Cancer. 2012;12(3):156-63.

[4] Sung GT, Gill IS. Robotic laparoscopic surgery: a comparison of the da Vinci and Zeus systems. Urology. 2001;58(6):893-8.

[5] Corcione F, Esposito C, Cuccurullo D, Settembre A, Miranda N, Amato F, et al. Advantages and limits of robot-assisted laparoscopic surgery: preliminary experience. Surg Endosc. 2005;19(1):117-9.

[6] Lanfranco AR, Castellanos AE, Desai JP, Meyers WC. Robotic surgery: A current perspective. Ann Surg. 2004;239(1):14-21.

[7] Hannaford B, Rosen J, Friedman DW, King H, Roan P, Lei C, et al. Raven-II: An open platform for surgical robotics research. IEEE Trans

Biomed Eng. 2013;60(4):954-9.

[8] Heemskerk J, Bouvy ND, Baeten CG. The end of robot-assisted laparoscopy? A critical appraisal of scientific evidence on the use of robot-assisted laparoscopic surgery. Surg Endosc. 2014;28(4):1388-98.

[9] Howe RD, Matsuoka Y. Robotics for surgery. Annu Rev Biomed Eng. 1999;1:211-240.

[10] Sullivan MJ, Frost EA, Lew MW. Anesthetic care of the patient for robotic surgery. Middle East J Anesthesiol. 2008;19(5):967-82.

[11] Kwoh YS, Hou J, Jonckheere EA, Hayati S. A Robot with Improved Absolute Positioning Accuracy for CT Guided Stereotactic Brain Surgery. IEEE Trans Biomed Eng. 1988;35(2):153-60.

[12] Satava RM. Surgical robotics: The early chronicles - A personal historical perspective. Surg Laparo Endo Per. 2002;12(1):6-16.

[13] Pransky J. ROBODOC - Surgical robot success story. Ind Robot. 1997;24(3):231-3.

[14] Kraft BM, Jager C, Kraft K, Leibl BJ, Bittner R. The AESOP robot system in laparoseopic surgery - Increased risk or advantage for surgeon and patient? Surg Endosc. 2004;18(8):1216-23.

[15] INTUITIVE SURGICAL AND COMPUTER MOTION ANNOUNCE MERGER AGREEMENT [http://sec.edgar-online.com/intuitive-surgical-inc/8-k-current-report-filing/2003/03/07/Section10.aspx]

[16] A Brief History of Robotic Surgery [http://hoffroboticsurgery.com/roboticsurgery.html]

[17] Robotics: the Future of Minimally Invasive Heart Surgery [http://biomed.brown.edu/Courses/BI108/BI108_2000_Groups/Heart_Surgery/Robotics.html]

[18] NEEMO 7: NASA'S Undersea Robotic Telemedicine Experiment [http://www.space.com/445-neemo-7-nasa-undersea-robotic-telemedicine-experiment.html]

[19] The da vinci surgery experience: over the past decade, more than 1.5 million surgeries have been performed worldwide using the da Vinci Surgical System [http://www.davincisurgery.com/assets/docs/da-vinci-surgery-fact-sheet-en-1005195.pdf?location=1&version=b]

[20] Tracking the Rise of Robotic Surgery for Prostate Cancer [http://www.cancer.gov/about-cancer/treatment/research/rise-robotic-surgery]

[21] da Vinci Surgical Robot Complaints on the Rise; Lawsuits Begin [http://olsmanlaw.com/main/da-vinci-surgical-robot-complaints-on-the-rise-lawsuits-begin/]

[22] Cardiac Surgery in the Age of IT [http://www.medicaldevice-network.com/features/feature106713/feature106713-3.html]

[23] da Vinci Si System [https://intuitivesurgical.com/company/media/images/davinci_si_images.php]

[24] Simon D. 4th biennial North American Summer School on Surgical Robotics, 21-25 July 2014

[25] Hands-On-Throttle-And-Stick

[http://falcon4.wikidot.com/avionics:hotas]

[26] da Vinci Xi System [https://www.intuitivesurgical.com/company/media/images/da-vinci-xi/]

[27] Memon S, Heriot AG, Murphy DG, Bressel M, Lynch AC. Robotic versus laparoscopic proctectomy for rectal cancer: a meta-analysis. Ann Surg Oncol. 2012;19(7):2095-101.

[28] Rozet F, Jaffe J, Braud G, Harmon J, Cathelineau X, Barret E, et al. A direct comparison of robotic assisted versus pure laparoscopic radical prostatectomy: a single institution experience. J Urol. 2007;178(2):478-82.

[29] Heemskerk J, de Hoog DE, van Gemert WG, Baeten CG, Greve JW, Bouvy ND. Robot-assisted vs. conventional laparoscopic rectopexy for rectal prolapse: a comparative study on costs and time. Dis Colon Rectum. 2007;50(11):1825-30.

[30] Morino M, Pellegrino L, Giaccone C, Garrone C, Rebecchi F. Randomized clinical trial of robot-assisted versus laparoscopic Nissen fundoplication. Br J Surg. 2006;93(5):553-8.

[31] Breitenstein S, Nocito A, Puhan M, Held U, Weber M, Clavien PA. Robotic-assisted versus laparoscopic cholecystectomy: outcome and cost analyses of a case-matched control study. Ann Surg. 2008;247(6):987-93.

[32] Park JS, Choi GS, Lim KH, Jang YS, Jun SH. S052: a comparison of robot-assisted, laparoscopic, and open surgery in the treatment of

rectal cancer. Surg Endosc. 2011;25(1):240-8.

[33] Magrina JF, Zanagnolo V, Noble BN, Kho RM, Magtibay P. Robotic approach for ovarian cancer: perioperative and survival results and comparison with laparoscopy and laparotomy. Gynecol Oncol. 2011;121(1):100-5.

[34] Sarlos D, Kots L, Stevanovic N, Schaer G. Robotic hysterectomy versus conventional laparoscopic hysterectomy: Outcome and cost analyses of a matched case–control study. Eur J Obstet Gynecol Reprod Biol. 2010;150(1):92-6.

[35] Link RE, Bhayani SB, Kavoussi LR. A prospective comparison of robotic and laparoscopic pyeloplasty. Ann Surg. 2006;243(4):486-91.

[36] Bell MC, Torgerson J, Seshadri-Kreaden U, Suttle AW, Hunt S. Comparison of outcomes and cost for endometrial cancer staging via traditional laparotomy, standard laparoscopy and robotic techniques. Gynecol Oncol. 2008;111(3):407-11.

[37] Catchpole K. Human factors and outcomes in pediatric cardiac surgery. In: Barach P, Jacobs J, Lipshultz SE, Laussen P, editors. Pediatric and Congenital Cardiac Care. London: Springer; 2015. p. 367-76.

[38] Lowndes BR, Hallbeck MS. Overview of human factors and ergonomics in the OR, with an emphasis on minimally invasive surgeries. Human Factors and Ergonomics in Manufacturing & Service Industries. 2014;24(3):308-17.

[39] Lönnerfors C, Persson J. Robot-assisted laparoscopic myomectomy; a

feasible technique for removal of unfavorably localized myomas. Acta Obstet Gyn Scan. 2009;88(9):994-9.

[40] van den Bedem L, Rosielle N, Steinbuch M. Design of Slave Robot for Laparoscopic and Thoracoscopic Surgery. International Conference of Society for Medical Innovation and Technology (SMIT), 28-30 Aug. 2008. p. 28-30.

[41] Branco AW, Kondo W, Stunitz LC, Filho AJB. Transumbilical laparoscopic bilateral nephrectomy. Brazilian Journal of Videoendoscopic Surgery. 2009;2(1):42-8.

[42] Raghupathi L, Grisoni L, Faure F, Marchal D, Cani MP, Chaillou C. An intestinal surgery simulator: Real-time collision processing and visualization. IEEE Trans Vis Comput Gr. 2004;10(6):708-18.

[43] Dachs GW, Peine WJ. A novel surgical robot design: minimizing the operating envelope within the sterile field. IEEE EMBS Annual International Conference. 31 Aug.-3 Sept. 2006. Article No. ThC06.1.

[44] Esposito MP, Ilbeigi P, Ahmed M, Lanteri V. Use of fourth arm in da Vinci robot-assisted extraperitoneal laparoscopic prostatectomy: Novel technique. Urology. 2005;66(3):649-52.

[45] Gomez JB, Ceballos A, Prieto F, Redarce T. Mouth gesture and voice command based robot command interface. IEEE International Conference on Robotics and Automation (ICRA), 12-17 May. 2009. p. 333-8.

[46] King BW, Reisner LA, Pandya AK, Composto AM, Ellis RD, Klein MD. Towards an autonomous robot for camera control during

laparoscopic surgery. J Laparoendosc Adv Surg Tech. 2013;23(12):1027-30.

[47] Nishikawa A, Hosoi T, Koara K, Negoro D, Hikita A, Asano S, et al. FAce MOUSe: A novel human-machine interface for controlling the position of a laparoscope. IEEE Trans Robot Autom. 2003;19(5):825-41.

[48] Cao Y, Miura S, Kobayashi Y, Kawamura K, Sugano S, Fujie MG, et al. Pupil variation applied to the eye tracking control of an endoscopic manipulator. IEEE Robot Autom Letters. 2016;1(1):531-8.

[49] Zinchenko K, Wu CY, Song KT. A Study on Speech Recognition Control for a Surgical Robot. IEEE Trans Ind Inform. 2016; Accepted.

[50] Kawai T, Fukunishi M, Nishikawa A, Nishizawa Y, Nakamura T. Hands-free interface for surgical procedures based on foot movement patterns. Engineering in Medicine and Biology Society (EMBC), 26-30 Aug. 2014. p. 345-8.

[51] Kim S, Kim Y, Kim H, Kim HC, Park YH, Lee C, et al. Surgical-Operation-By-Wire Type Surgical Operation Apparatus. U.S. Patent US20140243887 A1, issued August 28, 2014.

[52] Andrade L, Tenning C. Design of the Boeing 777 electric system. IEEE National Aerospace and Electronics Conference (NAECON), 18-22 May. 1992. p. 1281-90.

[53] Millard DJ. Fly by wire control-system. Aircr Eng Aerosp Tec. 1972;44(8):4-7.

[54] Burns BRA. Fly-by-wire and control configured vehicles - Rewards

and risks. Aeronaut J. 1975;79(770):51-8.

[55] From cable controlled flight controls to FBW [http://asn-xp.aerosoft.com/?page_id=3826.pdf]

[56] Wortman TD, Mondry JM, Farritor SM, Oleynikov D. Single-site colectomy with miniature in vivo robotic platform. IEEE Trans Biomed Eng. 2013;60(4):926-9.

[57] Noonan DP, Mylonas GP, Darzi A, Yang GZ. Gaze contingent articulated robot control for robot assisted minimally invasive surgery. IEEE/RSJ International Conference on Robots and Systems (IROS), 22-26 Sept. 2008. p. 1186-91.

[58] Gerard MJ, Armstrong TJ, Franzblau A, Martin BJ, Rempel DM. The effects of keyswitch stiffness on typing force, finger electromyography, and subjective discomfort. Am Ind Hyg Assoc J. 1999;60(6):762-9.

[59] Monika EH, Hubert S, Myriam JC. Robotics in General Surgery. In: Kim KC, editors. Introduction to the Robotic System. New York: Springer; 2014. p. 9-15.

[60] Kim M, Lee C, Park WJ, Suh YS, Yang HK, Kim HJ, et al. A development of assistant surgical robot system based on surgical-operation-by-wire and hands-on-throttle-and-stick. Biomed Eng Online. 2016;15:58.

[61] Kyriakis-Bitzaros ED, Stathopoulos NA, Pavlos S, Goustouridis D, Chatzandroulis S. A reconfigurable multichannel capacitive sensor array interface. IEEE Trans Instrum Meas. 2011;60(9):3214-21.

[62] Vandenberghe L, Boyd S, El Gamal A. Optimizing dominant time constant in RC circuits. IEEE Trans Comput-Aided Des Integr Circuits Syst. 1998;17(2):110-25.

[63] Maeno T, Kawamura T. Geometry design of an elastic finger-shaped sensor for estimating friction coefficient by pressing an object. IEEE International Conference on Robotics and Automation, 14 Sep. 2003 p. 1533-8.

[64] Abbott DJ, Becke C, Rothstein RI, Peine WJ. Design of an endoluminal NOTES robotic system. International Conference on Intelligent Robots and Systems (IROS), 29 Oct.-2 Nov. 2007. p. 410-6.

[65] Lee C, Park YH, Yoon C, Noh S, Lee C, Kim Y, et al. A grip force model for the da Vinci end-effector to predict a compensation force. Med Biol Eng Comput. 2015;53(3):253-61.

[66] Serdar Kucuk ZB: Robot Kinematics: Forward and Inverse Kinematics. In Industrial Robotics: Theory, Modeling and Control.

[67] Wang YM, Li Y, Zheng JB. A camera calibration technique based on OpenCV. International Conference on Information Sciences and Interaction Sciences (ICIS), 23-25 Jun. 2010. p. 403-6.

[68] Zou L, Li Y. A method of stereo vision matching based on OpenCV. International Conference on InAudio Language and Image Processing (ICALIP), 23-25 Nov. 2010. p. 185-90.

[69] Peter JH, Ellison EC, Innes JT, Liss JL, Nichols KE, Lomano JM, et al. Safety and efficacy of laparoscopic cholecystectomy. A

prospective analysis of 100 initial patients. Ann Surg. 1991;213(1):3.

[70] Shin WH, Kwon DS. Surgical robot system for single-port surgery with novel joint mechanism. IEEE Trans Biomed Eng. 2013;60(4):937-44.

[71] Joseph R, Goh A, Cuevas S, Donovan M, Kauffman M, Salas N, et al. Chopstick surgery: a novel technique improves surgeon performance and eliminates arm collision in robotic single-incision laparoscopic surgery. Surg Endosc. 2010;24(6):1331-5.

[72] Sen Gupta G, Mukhopadhyay SC, Messom CH, Demidenko SN. Master-slave control of a teleoperated anthropomorphic robotic arm with gripping force sensing. IEEE Trans Instrum Meas. 2006;55(6):2136-45.

[73] Persson PO, Strang G. Smoothing by Savitzky-Golay and Legendre filters. In: Rosenthal J, Gilliam DS, editors. Mathematical Systems Theory in Biology, Communications, Computation, and Finance. New York: Springer; 2003. p. 301-15.

[74] Liu D, Li J, He C, Kong K. Workspace analysis based port placement planning in robotic-assisted cholecystectomy. International Symposium on IT in Medicine and Education (ITME), 9-11 Dec. 2011. p. 616-20.

[75] Kim KY, Song HS, Suh JW, Lee JJ. A novel surgical manipulator with workspace-conversion ability for telesurgery. IEEE/ASME Trans Mechatronics. 2013;18(1):200-11.

[76] Markvicka E, Lackas K, Frederick T, Bartels J, Farritor S, Oleynikov

D. Gross Positioning System for In Vivo Surgical Devices. J Med Dev. 2013;7(3):030922.

[77] Haidegger T, Kovács L, Precup RE, Benyó B, Benyó Z, Preitl S. Simulation and control for telerobots in space medicine. Acta Astronaut. 2012;81(1):390-402.

[78] Gupta V, Reddy NP, Batur P. Forces in surgical tools: Comparison between laparoscopic and surgical forceps. Annual International Conference of the IEEE Engineering in Medicine and Biology Society (EMBS), 31 Oct.-3 Nov. 1996. p. 223-4.

[79] Sukthankar SM, Reddy NP. Towards force feedback in laparoscopic surgical tools. Annual International Conference of the IEEE Engineering in Medicine and Biology Society (EMBS), 3-6 Nov. 1994. p. 1041-2.

[80] Jordán S, Takács A, Rudas I, Haidegger T. Modelling and control framework for robotic telesurgery. Third Joint Workshop on New Technologies for Computer/Robot Assisted Surgery, 11-13 Sept. 2013. p. 89-92.

[81] Takács Á, Kovács L, Rudas IJ, Precup RE, Haidegger T. Models for Force Control in Telesurgical Robot Systems. Acta Polytechnica Hungarica. 2015;12(8):95-114.

[82] Lum MJ, Rosen J, King H, Friedman DC, Lendvay TS, Wright AS, et al. Forces in surgical tools: Comparison between laparoscopic and surgical forceps. Annual International Conference of the IEEE Engineering in Medicine and Biology Society (EMBS), 3-6 Sept.

2009. p. 6860-3.

[83] Xu S, Perez M, Yang K, Perrenot C, Felblinger J, Hubert J. Determination of the latency effects on surgical performance and the acceptable latency levels in telesurgery using the dV-Trainer® simulator. Surg Endosc. 2014;28(9):2569-76.

[84] Cadiere GB, Himpens J, Germay O, Izizaw R, Degueldre M, Vandromme J, et al. Feasibility of robotic laparoscopic surgery: 146 cases. World J Surg. 2001;25(11):1467-77.

[85] Lee C, Kim M, Kim YJ, Hong N, Ryu S, Kim S, et al. Soft robot review. Int J Control Autom Syst. 2017;15(1):3-15.

국문초록

기존 개복 수술의 단점을 극복하기 위해 최소 침습 수술이 개발되었으며, 이러한 최소 침습 수술에도 존재하는 한계를 해결하고자 로봇을 이용한 복강경 수술이 널리 시행되고 있다. 하지만 로봇 수술은 기존 보다 큰 수술실 공간을 필요로 하고 수술실 내부 환경의 복잡도를 증가시키는 등의 문제를 야기하는데, 이들은 여전히 극복되어야 하는 상태이다.

이를 위해 본 연구에서는 기존 복강경 수술 로봇 마스터 인터페이스에 부가적인 기능을 수행할 수 있는 인터페이스를 추가하여 해결책을 제시하고자 하며, 항공우주공학에서 널리 사용되고 있는 Hands-On-Throttle-And-Stick (HOTAS) 기법을 복강경 수술 로봇에 접목시키고자 한다. 이는 항공기에서 HOTAS 사용으로 인해 교전 중 시선을 아래로 향하지 않고서도 비행과 무장, 레이더 조작 등이 가능해졌을 뿐 아니라 그에 따라 항공기 조종석 내부 인원이 두 명에서 한 명으로 감소되었고, 이로 인해 조종석 내부의 복잡도 또한 대폭 감소된 효과를 복강경 수술 로봇을 위한 수술실 환경에서 또한 적용시키기 위함이다.

따라서 본 연구에서는 두 종류의 추가적인 인터페이스를 제안하였으며, 이들은 모두 da Vinci Research Kit의 Mater Tool Manipulator에 설치되어, 수술자의 검지를 이용해 부가적인 기능을 간편하게 수행 가능하도록 설계 및 개발되었다. 첫 번째로는 다 방향 스위치와 무선 통신 모듈을 이용해 제작된 9-way Compact HOTAS, Novel Master Interface (NMI)을 연구 및 개발하였다. 다 방향 스위치를 이용해 수술자가 의도를 전달할 수 있도록

하였으며, 반응 시간, 전력 소모 등 실험을 거쳐 효용성을 입증하였다. 두 번째로, 보다 직관적이고 편리한 조작을 위해 정전식 터치 방식을 도입하여 Capacitive Touch Type Compact HOTAS인 improved Novel Master Interface (iNMI)을 연구 개발하였다. 정전식 터치 제어 방식을 통해 수술자가 의도를 보다 직관적이고 편리하게 전달할 수 있도록 하였으며, 다수의 반복 실험을 통해 효용성을 입증하였다.

뿐만 아니라, 이러한 추가적인 인터페이스를 통해 복강경 수술 로봇 시스템의 활용도를 상승시키고자 아래와 같이 두 종류의 응용시스템을 제안하였으며, 이들은 항공우주공학의 Fly-By-Wire 기법을 수술 로봇에 접목시킨 Surgical-Operation-By-Wire 기법을 기반으로 연구 및 개발되었다.

첫 번째로, 추가적인 인터페이스에 의해 제어될 수 있는 Robotic Assistant를 개발하였다. 이는 수술자가 수술 도중 보조의사의 업무를 직접 수행할 수 있도록 하기 위함인데, 이러한 방법은 보조의사와의 지속적인 의사소통으로 인해 발생하는 피로도 증가를 방지하고자 하였을 뿐 아니라, 숙달되지 않은 보조의사 혹은 수술자와 보조의사 간의 의사소통 및 의도전달 문제로 인해 발생할 수 있는 수술기구 간 충돌 또한 방지하고자 하였다. 고안한 시스템은 두 개의 추가적인 인터페이스, 보조 수술기구, 그리고 6축 로봇 팔로 구성되어있다. 보조 수술기구는 1,000번의 사용에도 집는 힘이 일정한 것으로 확인되었으며, 반응시간은 0.4초로 계산되어 사람이 손쉽게 적응할 수 있는 반응시간으로 확인할 수 있었다. 시스템의 동작 범위는 8,397.4 cm^3로 계산되어 다양한 종류의 수술을 시행할 수 있을 것으로 판단되었으며, 본 시스템을

처음 접하는 참가자가 술기 테스트에서 제한시간 내에 임무를 수행하여 시스템이 잘 구성되었음을 확인하였다.

두 번째로, 수술자가 수술도중 수술기구와 복강경을 함께 제어할 수 있도록 무선 인터페이스를 통해 제어가 가능한 스테레오 복강경 시스템을 개발하였다. 이는 기존 수술 로봇 시스템에서 복강경 제어를 위해 수술기구에 대한 제어 권한을 포기함으로 인해 발생하는 불연속적인 수술 흐름을 극복하기 위함이며, 이로 인해 발생하였던 수술 시간 증가, 수술기구 간 충돌, 그리고 내부 장기 손상 등 문제를 해결하고자 하였다. 제안한 시스템은 두 개의 추가적인 인터페이스, 4 자유도 복강경 제어 시스템, 그리고 스테레오 복강경으로 구성되어있다. 본 시스템을 처음 접하는 참가자가 시스템의 성능 평가를 위해 설계된 술기 테스트를 제한시간 내 수행하는 것을 확인하였으며, 기존 가설에 따라 문제점을 극복하는 것을 확인하였다. 또한 시스템의 동작 범위는 20,378.3 cm^3로 계산되어, 많은 종류의 수술에 적합하다고 판단되었다.

다양한 검증을 통해 제안한 추가적인 인터페이스가 장착된 수술 로봇 시스템이 기존 로봇 수술의 여러 한계점을 극복할 수 있는 것으로 확인하였다.

핵심어: 복강경 수술 로봇, 추가적인 master interface, 호타스 조종간, 보조 수술 로봇, 스테레오 복강경 시스템, 전기신호식 수술 로봇 제어.
학번: 2013-21032